ForWind
Zentrum für Windenergieforschung
Bremen
Hannover
Oldenburg

Leibniz
Universität
Hannover

Probabilistic Safety Assessment of Offshore Wind Turbines

Annual Report 2013

7th February 2014

Cover: Windturbines on the ocean © Zentilia

Research Project:	Probabilistic Safety Assessment of Offshore Wind Turbines (PSA) Probabilistische Sicherheitsbewertung von Offshore-Windenergieanlagen (PSB)
Sponsored by:	Ministry for Science and Culture in Lower Saxony Niedersächsisches Ministerium für Wissenschaft und Kultur
Support Code:	GZZM2547
Research Period:	01.12.2009 – 30.11.2014
Reference Period:	01.12.2012 – 30.11.2013
Homepage:	www.psb.uni-hannover.de

All institutes are members of ForWind and belong to the Leibniz Universität Hannover:

Institute of Concrete Construction
Prof. Dr.-Ing. Steffen Marx / Dr.-Ing. Michael Hansen (Coordination)

Institute of Building Materials Science
Prof. Dr.-Ing. Ludger Lohaus

Franzius Institute of Hydraulics, Waterways and Coastal Engineering
Prof. Dr.-Ing. habil. Torsten Schlurmann

Institute for Geotechnical Engineering
Prof. Dr.-Ing. Martin Achmus

Institute for Steel Construction
Prof. Dr.-Ing. Peter Schaumann

Institute of Structural Analysis
Prof. Dr.-Ing. habil. Raimund Rolfes

Institute for Drive Systems and Power Electronics
Prof. Dr.-Ing. Axel Mertens / Prof. Dr.-Ing. Bernd Ponick

Institute of Electric Power Systems
Prof. Dr.-Ing. habil. Lutz Hofmann

Institute for Machine Design and Tribology
Prof. Dr.-Ing. Gerhard Poll

Insitute of Turbomachinery and Fluid Dynamics
Prof. Dr.-Ing. Jörg Seume

Content

1 Introduction 1

2 Work Packages (WP) 4

2.1 Safety of Offshore Wind Turbines (WP 1) 4

2.2 Action Effects of Wind and Waves (WP 2) 6

2.3 Soil (WP 3) 15

2.4 Foundation and Support Structure (WP 4) 22

2.5 In-Situ Assembly (WP 5) 31

2.6 Monitoring of Mechanical Components (WP 6) 36

2.7 Diagnostic Systems for Electronic Systems (WP 7) 44

2.8 Reliability of the Grid Connection (WP 8) 51

3 Summary 56

4 Literature 58

4.1 Publication List 58

4.2 Doctoral, Diploma, Master and Bachelor Theses 59

1 Introduction

Institute of Concrete Construction
Michael Hansen, Boso Schmidt

The ForWind research project Probabilistic Safety Assessment of Offshore Wind Turbines (PSA OWT) is sponsored by the Ministry for Science and Culture in Lower Saxony since 1.12.2009. In this research project safety assessments of the support structure and specific electrical and mechanical components of Offshore Wind Turbines (OWT) are performed. Since 2010 project descriptions, objective targets and research results are documented in annual reports which are available on www.psb.uni-hannover.de. PSB Annual Report 2013 contains assumptions, aims and outcomes for several examinations concerning parts of OWT in view of civil engineering, mechanical engineering and electrical engineering.

Within this research project in several work packages (WP) a wide variety of topics concerning probabilistic methods are analysed. These methods and further correlations partially were described in WP 1 in former annual reports. Furthermore, connections between the involved institutes and their treated subjects are shown in this coordinating WP1.

Extreme hydrodynamic loads on OWTs result from breaking waves, which cause severe impact on offshore structures and induce significant singular stresses as well as vibration and therefore discrete degradation of the support structure. For an efficient design of OWTs, dominant and significant sea state parameters as well as wave-breaking probabilities must be considered. This work is done in the first part of WP2. In the first step design wave heights and occurrence of wave trains in the North Sea have been analysed on the basis of statistical analysis of extreme events. The second step deals with the wave-breaking probability, which is investigated by means of laboratory experiments in two-dimensions to quantify the scatter of the influencing factors, i.e. significant wave height H_S, peak period T_P, random phase angle φ and water depth d. The laboratory experiments show a significant influence of the random phase angle, i.e. wave sequence in the time series, on the wave-breaking probability, which has to be investigated in depth in further test runs.

In the second part of WP2 wind forces are examined. In addition to the complex flow environment and the geometric deviations, structural imperfections of rotor blades are one of the main sources of uncertainties in wind turbine design. These can arise due to imperfections of the composite materials, which can be caused by variations of the fiber and matrix material properties and the fiber volume ratio etc. Structural uncertainties can also arise due to tolerances in the non-automated manufacturing process. In order to investigate the effect of structural uncertainties on the full-system mode shapes and natural frequencies of an offshore wind turbine (OWT), the distributed blade mass density and the cross-sectional flapwise and edgewise stiffness are varied relatively with respect to the corresponding baseline parameters. The variations of the spatially correlated structural properties are modelled by a random field approach. The results show a significant scatter of the natural frequencies of the rotor modes and the torsional drivetrain mode which can lead to an increased risk for resonances with the 3P harmonics of the rotational speed.

WP 3 deals with the calculation of partial safety factors for mainly axially loaded offshore foundation piles. Therefore a case study of a Reliability Based Design for two common soil profiles and two design methods, the API-method and the ICP-method, was performed. Moreover a calibration of partial safety factors was carried out to match the safety requirements of the Eurocode 0. According to the computed results the partial safety factors should be decreased

for the API-method, where an increase for the ICP-method seems to be suitable. Thereby also a more accurate determination of the required embedded pile length was achieved compared to deterministic design.

The foundation and support structures of OWT are examined in WP4. Reliability analyses are carried out for a monopile and jacket structure. Limit states which are critical for the structural design of OWTs are identified. On basis of the ultimate limit state as defined by valid standards, extreme events as well as the statistical properties of the resulting loads acting on substructures are investigated. Especially the scattering of the environmental conditions which describe the sea state and wind fields are considered within the ongoing research. Also, the correlation between parameters has to be taken into account for the probabilistic design. Different methods such as the Monte-Carlo simulation can be applied in order to determine the probability of failure for scattering parameters. In addition, the fatigue limit state has to be considered for branched structures such as jackets and tripods. Here, the fatigue damage is investigated concerning its statistical properties.

In WP 5 risk factors of grouted joints during the execution process are investigated by using methods like Preliminary Hazard Analysis (PHA) and Fault Tree Analysis (FTA). First, supporting structures and typical offshore boundary conditions were analysed. To perform a detailed PHA, the different commonly used supporting structures under typical offshore conditions were analysed according to the load bearing behaviour. Based on the findings of the PHA, different failure modes of the grouting process were simulated using several laboratory testing facilities. These tests simulate possible adverse effects and their influence on the strength of the hardened grout material. In a subsequent FTA, the main risk factors according to the load bearing capacity of the grouted joint will be identified. The findings will be used to develop recommendations to minimise the risk for possible defects of the grouted connection.

Drive trains of wind power plants contain different mechanical components with limited lifetimes which can only be estimated for selected types of failures. For example, rolling element bearings are exposed to operation conditions causing damage mechanism that aren't fully investigated yet and still missing in common calculations of bearing lifetime. To nevertheless ensure a high availability and low maintenance costs, maintenance has to be planned early and effective, especially for hard to reach OWT, by an early detection of failures during operation. WP6 therefore deals with the development and testing of condition monitoring systems for large size rolling element bearings. The measurement of vibration signals emitted by a repetitive overrolling of failures in the raceways of rolling element bearings and a novel method for signal analysis and evaluation are tested on a large size bearing test rig as well as on a real wind turbine.

WP7 focuses on the online fault detection in electrical machines using search coil systems. All important types of faults and damages in electrical machines result in characteristic changes of the magnetic air-gap field. These changes can be used to detect a fault by search coils placed in the stator slots based on the voltage induced in them to identify the type of fault in dependence of the frequency. Search coil systems are especially suitable for the detection of interturn faults and eccentricities, since these faults have no or little influence on the quantities at the terminals of a machine and are therefore not easy to be detected from the outside. Based on previous researches of search coil systems for synchronous machines, the special challenges of the design of search coil systems for permanent magnet synchronous machines with high pole

pair/slot number combinations are determined. In this respect different approaches for the design of search coil systems are presented. Furthermore, design rules for search coil systems in multi-pole permanent magnet synchronous machines are developed.

The converter lifetime of wind turbines is addressed in the first part of WP 8. Lifetime simulation models have been built. In 2013 they have been extended to dynamic operation mode and a complete simulation model was built. Real wind speed characteristics are integrated in the model. The thermal behaviour of the power electronics is modelled. First results show the dynamic thermal load of the converters for real wind speed steps.

For a reliability analysis of grid connections of offshore wind farms, different grid topologies and grid structures are analyzed and evaluated concerning their reliability in the second part of WP 8. On this occasion the uppermost purpose is to determine which grid topology owns the highest reliability. As input quantities for the reliability analysis of wind farm connections, characteristic reliability parameters of electrical components like transformers, cables etc. are considered. A model for probabilistic analysis for probabilistic reliability analysis for the entire wind farms including the grid connection was created. This model performs simulations under variation of reliability parameters. Thus potential weaknesses of grid connections are identified. But also profit calculations and location assessments are possible.

2 Work Packages (WP)

2.1 Safety of Offshore Wind Turbines (WP 1)

Institute of Concrete Construction
Michael Hansen, Boso Schmidt

2.1.1 Motivation

Within the last three Annual Reports [1]-[3] basics for the used methods and justified approaches were documented. Involved WPs take different methods for reliability analysis to reach their special aims. But some objectives respectively assumptions are quite similar for each WP. Therefore, it seems to be acceptable and even necessary to unite these assumptions into principles. Thus, a database with justified parameters was created.
An ongoing discussion deals with the target reliability of components and whole structures [4]. There is still no predefined value for the acceptable possibility of failure respectively the so-called reliability index, cf. Annual Report 2012 [1]. Nevertheless, in some investigations we need a limit value. Hence, for example in WP 4 a value is defined with respect to standard although these values are controversially discussed. Even critical limit states within the considered tasks are not easy to define. Hence, the researchers pick out comprehensible parts and examine relevant parameters and correlations.
The used methodology and some determined results in the WP are shown in this Annual Report 2013.

2.1.2 Approach

In WP1 one objective target is to unite the methodology in all WPs. Therefore, regularly meetings with participation of all involved persons were held about all 10 weeks since project start. Scheduled short presentations of each WP make sure that individual approaches could be discussed. Thus, common assumptions based on a coordinated method of investigation were found. These assumptions were clarified and validated at two workshops held in 2012, cf. Annual Report 2012 [1] paragraph 2.1.3.
Additionally, in bilateral discussions [5] the proceedings in each WP were evaluated. Goal and purpose of these dialogues was to develop commonalities between the used methods and input variables in different WPs. The networking of each WP within the whole project was examined, too. By this possible cooperation and similar works were detected.

2.1.3 State of work

The outcomes of the bilateral discussions were documented [5]. Furthermore, in regular meetings the works and problems within the several work packages are discussed. The networking between the WPs has a high priority. Thus, within WP1 possible similar works of the individual WPs are detected. The persons dealing with these WP try to obtain benefits by comparing their proceedings.

The results of this comprehensive research project shall be documented in reviewed papers. In successive journal issues all WPs will be presented with their link to each other. Therefore, a frame for these publications is arranged at present.

References

[1] PSB-OWEA – Annual Report 2012. Hannover, 2013.

[2] PSB-OWEA – Annual Report 2011. Hannover, 2012.

[3] PSB-OWEA – Annual Report 2010. Hannover, 2011.

[4] Bericht Nr. 1149 Teil 2: Zielzuverlässigkeiten, Systemwahrscheinlichkeiten und Kombination der Einwirkungen Wind und Welle – Grundlagen. Interner Bericht, Institut für Massivbau, Leibniz Universität Hannover, Januar 2012.

[5] Bericht Nr. 1149 Teil 6: Zusammenfassung der bilateralen Gespräche zwischen Teilprojekt 1 und allen weiteren Teilprojekten. Interner Bericht, Institut für Massivbau, Leibniz Universität Hannover, November 2013.

2.2 Action Effects of Wind and Waves (WP 2)

Institute of Turbomachinery and Fluid Dynamics (TFD)
Benedikt Ernst, Joerg Seume

Franzius-Institute for Hydraulic, Waterways and Coastal Engineering (FI)
Mayumi Wilms, Arndt Hildebrandt,
Torsten Schlurmann

For offshore wind turbines (OWTs), aerodynamic wind loads and hydrodynamic wave loads are essential input parameters for probabilistic investigations. Therefore, in this work package characteristic parameters of the loads and the resistance of OWTs will be determined. As a common database, the wind and wave measurements at FINO 1 are used.

2.2.1 Motivation (TFD)

Offshore wind turbines operate in a complex unsteady flow environment which causes fluctuating aerodynamic loads. The unsteady flow environment is characterized by a high degree of uncertainty. In addition, manufacturing tolerances and material imperfections also cause uncertainties in the design process.
The rotor blades of wind turbines are long, slender, and flexible structures and future rotor blades tend to become even longer and more slender. For these structures the consideration of uncertainties and aeroelastic phenomena becomes increasingly important with regard to fatigue strength and overall performance.
In order to consider uncertainties in the design phase of OWTs, probabilistic design methods can be used. This will lead to cost-optimized OWTs with acceptable reliability and safety levels.

2.2.2 Approach (TFD)

In this part of the work package, the failure probability of rotor blades of OWTs due to fatigue and ultimate loading will be investigated. In order to do so, 3D turbulent stochastic wind fields are generated based on the FINO 1 data. The aim is to investigate the impact the wind field parameters on the aeroelastic behavior of OWTs and on the probability of failure. Furthermore, the sensitivity of the loads and the eigenfrequencies due to variations of material and/or geometric properties are investigated.
For the investigations, the aeroelastic model of a 5 MW OWT [1], which was developed at the National Renewable Energy Laboratory (NREL), is used. The wind fields are generated by the simulation software TurbSim [2] and the turbine response is computed with the aeroelastic simulation software FAST [3].

2.2.3 State of Work (TFD)

Structural uncertainty of rotor blades

In addition to the complex flow environment and the geometric deviations, structural imperfections of rotor blades are one of the main sources of uncertainties in wind turbine design. These can arise due to imperfections of the composite materials, which can be caused by variations of the fiber and matrix material properties and the fiber volume ratio etc. Structural uncertainties can also arise due to tolerances in the non-automated manufacturing process. As far as the authors know, detailed information about structural uncertainties and manufacturing tolerances of wind turbine rotor blades are not available in open literature.
In order to investigate the effect of structural uncertainties on the full-system mode shapes and natural frequencies of an OWT, the distributed blade mass density (BMassDen) and the cross-sectional flapwise (FlpStff) and edgewise stiffness (EdgStff) are varied relatively with respect to the corresponding baseline parameters (cf. Figure 1). The relative variations are described by a normal distribution ($\mu = 0\%$, $\sigma = 10\%$) and the relative parameter variations are created

simultaneously by means of a Latin hypercube sampling. It is assumed that the three parameters are independent from each other. However, there is a spatial dependency of the cross-sectional parameters along the blade radius (length). In order to investigate this, three different types of spatial variations are examined. First, it is assumed that the relative variations are uniformly distributed along the blade. Second, it is assumed that the parameters of a cross-section varies independently from other cross-sections. Third, it is assumed that the variations of the structural parameters are spatially correlated.

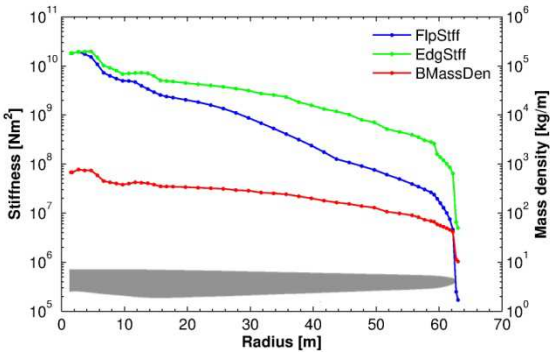

Figure 1: Blade mass density and cross-sectional stiffness parameters of the 5 MW OWT model [4] (data based on [1])

The variations of structural properties, which are spatially correlated, are modeled by a random field approach. The dependency structure between the random field values at different locations is described by the covariance matrix, which is based on an inverse-exponential correlation function with three different correlation lengths b: 10%, 50%, and 100% of the total blade length L. Finally, the random fields are created by means of the Karhunen-Loeve expansion which uses a spectral representation of the random field [6].

In case of a spatial uniform variation, the structural parameters are varied constantly along the rotor blade length. The spatial independent variation leads to complete random variations along the blade length which can cause local extreme fluctuations. These local fluctuations are damped if spatially correlated parameters are assumed. In case of a small correlation length, the correlation function goes quickly to zero and the spatial random field is weak/low correlated. For an increasing correlation length, the correlation increases and the variations along the blade become smoother, see e.g. [4, 5].

In order to investigate the effect of these structural parameter variations on the eigenfrequencies of the rotor blade and the full-system natural frequencies of the OWT model, a tool chain / simulation process was developed based on MATLAB, BModes [7], and FAST [3].

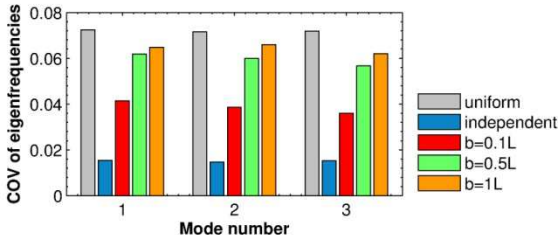

Figure 2: Coefficient of variation of the blade eigenfrequencies at standstill [4]

BModes uses a finite-element approach to calculate the mode shapes and eigenfrequencies of the rotor blade. The resulting scatter (coefficient of variation - COV) of the eigenfrequencies of the first three blade modes at standstill (without rotation), caused by the different types of spatial parameter variations, are shown in Figure 2. It can be seen that the highest COVs are caused by the spatial uniform variation of the blade parameters, while the spatial independent variation leads to the lowest COV. In this case, the effect of local variances can be compensated, which only leads to small variations of the eigenfrequencies. In terms of spatial correlated parameter variations an increasing correlation length leads to an increasing COV. This behavior can also be observed for natural frequencies of the rotor modes. For the correlation length

b = 0.1L, the COV is approximately in the middle between the two extremes, which are the spatially uniform and spatially independent variations. Based on this, b = 0.1L seems to be a reasonable assumption for subsequent studies.
For the design of the OWT it is necessary to consider aeroelastic effects on the entire structure, because the drivetrain and tower-nacelle subsystem of an OWT do not see the vibration of a single blade, instead these components see the modes of the entire rotor. In order to determine the system natural frequencies of the OWT model, the aeroelastic code FAST [3] is used to create the linearized state-space model and a multi-blade coordinate transformation is performed to capture the cumulative dynamics of all blades in a fixed (non-rotating) frame of reference [8]. The system natural frequencies and mode shapes are then calculated by means of an eigenanalysis.

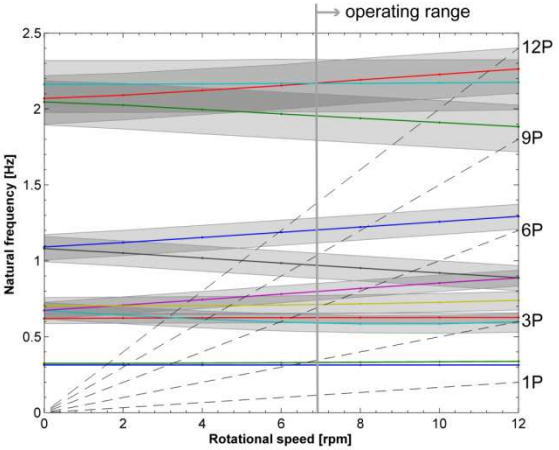

Figure 3: Campbell diagram of the OWT model [5]

The OWT model is a variable speed wind turbine. Therefore, the effect of structural uncertainty is investigated for different rotational speeds. Figure 3 shows the Campbell diagram with the first 11 modes. The grey shaded regions indicate the inter-quantile range which contains the middle 95% of all values. It is shown that the effect on the tower modes (mode 1 and 2) is very small, but there is a high frequency scatter of the rotor modes. The variations of the blade structural parameters also affects the drivetrain torsional mode (mode 3) which can lead to an increased risk for resonances with the 3P harmonics of the rotational speed.

Work in progress

Extreme loads

The IEC standards [9, 10] require to determine the extreme loads in an operating state with a recurrence period of 50 years by statistical extrapolation. Based on the work of Ernst and Seume [11], parameter studies will be performed to identify the most sensitive parameters and assumptions of the peak over threshold method.

Geometry and structural uncertainty

A combined analysis of structural and geometric uncertainties of the rotor blades will be performed to investigate the effect on the natural frequencies, loads, and overall performance of an OWT.

Probabilities of failure

In order to determine the probabilities of failure due to fatigue in normal operation, different types of limit state functions will be investigated. Furthermore, different reliability and Monte Carlo based methods will be used.

2.2.4 Motivation (FI)

Extreme hydrodynamic loads on OWTs result from breaking waves, which cause severe impact on offshore structures and induce significant singular stresses as well as vibration and therefore discrete degradation of the support structure. The relevant loads for a design base depend on the prevalent sea state (wave height) and geometry characteristics of breaking waves (intensity of impact) in a storm. All influencing factors vary significantly in the natural sea state. For an efficient design of OWTs, dominant and significant sea state parameters as well as wave-breaking probabilities must be considered.

2.2.5 Approach (FI)

In the first step, design wave heights and occurrence of wave trains in the North Sea have been analyzed on the basis of statistical analysis of extreme events. The second step deals with the wave-breaking probability, which is investigated by means of laboratory experiments in two-dimensions to quantify the scatter of the influencing factors. Factors considered here as influencing are: significant wave height H_S, peak period T_P, random phase angle φ and water depth d. The significant wave height H_S and peak period T_P characterise the sea spectrum, for example a JONSWAP spectrum for the North Sea. By means of the random phase angle φ, the sea spectrum (frequency domain) can be transformed to a water surface elevation time series.

The overall goal is to determine the sensitivity of wave-breaking probability to each input factor. In a first set of test runs, the influence of the factors significant wave heigth H_S and random phase angle φ is investigated.

2.2.6 State of Work (FI)

In the following, the test setup, test program and procedure, and the results of the selected tests are presented.

Test setup

The model tests were carried out in the wave flume of the Franzius-Institute (WKS), which has overall dimensions of 110 m length, 2.2 m width and 2.0 m height. The piston type wave maker is hydraulically driven and capable of generating regular and irregular waves

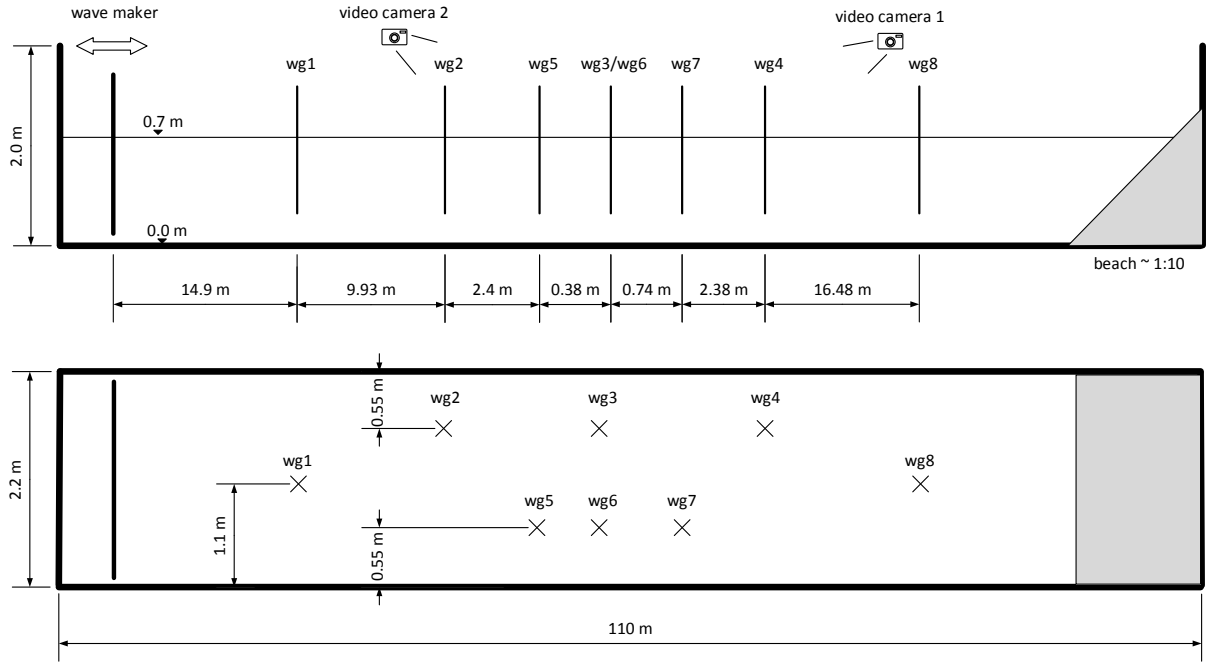

Figure 4: Sketch of the experimental setup in the WKS wave flume.Top: side view of setup. Bottom: top view of setup. wg: wave gauge

with wave heights up to 0.35 m while using a stroke of up to ±0.30 m by a water depth of up to 1.2 m. In the rear part of the flume, a beach is installed as a passive wave absorber in order to minimize reflections. For the tests, the water surface elevation were measured using eight capacitive type wave gauges installed along the flume and covering a testing area of 30 m. As additional measurement equipment, two video cameras were installed to record the tests and to determine the wave-breaking in post-processing. A sketch of the test setup is given in Fig. 4. The cameras were installed with such a viewing direction, so that they faced wave gauges WG2 to WG7, see Fig. 5 and Fig. 6.

Figure 5: Viewing direction of video camera 1 in the WKS wave flume

Figure 6: Viewing direction of video camera 2 in the WKS wave flume

Wave gauge WG1 were used to determine the incident wave spectrum. The position of testing area in the flume is a compromise between minimal distance to the wave maker (at least 5 times maximum wave length) and maximum distance to the beach (to avoid wave reflections in the testing area).

Test program and procedure

The model tests were carried out in a length scale of 1:40, which is a compromise between possible wave generation and possible water depths. After the wave gauges and the video cameras were installed, the flume was filled to still water level and kept constant at $d = 0.7$ m for all tests. A test program with eight tests were compiled, see table 1. As a spectrum, a narrow-band JONSWAP spectrum with enhancement factor $\gamma = 3.3$ were used. For all tests, the peak period was $T_P = 1.7$ s, number of generated waves was 50 and the wave maker theory was first order. In table 1 the random phase angle φ is indicated as “a”, “b” or “c”, and refers to three, fix sets of random phase angles, which were generated once before the tests were carried out and stored.

Table 1: Compilation of conducted model tests in the WKS wave flume

#	H_S [m]	random phase angle φ
1	0.2	a
2	0.2	a
3	0.2	b
4	0.2	b
5	0.2	a
6	0.2	c
7	0.225	a
8	0.25	a

That way, the wave spectrum, characterised with significant wave height H_S and peak period T_P, could be transformed repeatedly to time domain and resulting in the same wave train every time. This means, test number 1,2 and 5 are the same wave train, and test number 3 and 4 are the same wave train; they have the respective same significant wave height H_S and the same phase angle distribution. Those retests were done, to analyse the reproducibility of the wave trains and number of breaking waves accordingly.

During each test run, all wave gauges and video cameras were continuously

collecting data. The wave gauges have an analog output system (voltage outputs) and the data were sampled by a HBM analog-digital converter in digital form. For data storage, the HBM sampling and control software catmanEasy was used and Mathworks Matlab was used for post-processing.
A waiting time of at least 10 min between each test, ensured no remaining oscillations, thus no interference, from the previous test run.

Results

In a first step, the test runs were analysed in regard to plausibility (comparison of target value and actual value) and reproducibility (comparison of retests).
The analysis of plausibility shows a mean deviation of 3.5 % for the significant wave height H_S and a mean deviation of 1.8 % for the peak period T_P. Please note, that the actual measured significant wave height were determined in frequency domain with Fast Fourier Transform (FFT). The mean deviations are small and the targeted wave parameters are generated.
The analysis of reproducibility shows a mean coefficient of determination of R = 0.998 for test runs 1,2 and 5 and R = 0.997 for test runs 3 and 4. Fig. 7 shows exemplary the first 20 sec of the time series with H_S = 0.2 m and phase angle distribution “a”.

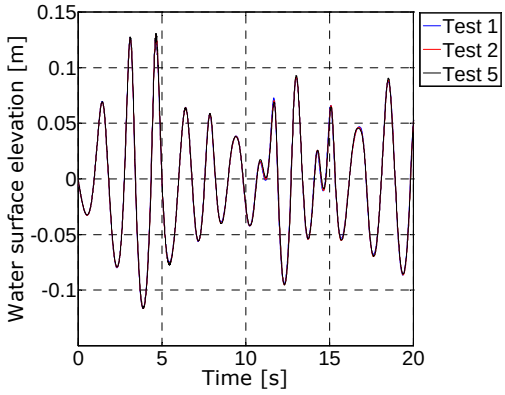

Figure 7: Reproducibility of test serie with H_S = 0.2 m and phase angle distribution "a"

The analysis shows that the time series can be reproduced very well and therefore the resulting numbers of breaking waves are reliable.
In a second step, the number of breaking waves were determined by re-watching the video camera data. The observed breakers were classified in “spilling breaker” and “whitecapping”.
In table 2, the results for the number of breaking waves are compiled with their respective time stamp in relation to the start of the wave maker. The results of the retests 2 and 5 are the same as for test 1, as well as the results for the retest 4 is the same as for test 3; the reproducibility is again verified, which is why the results for retests 2, 4 and 5 are not shown in table 2.

Table 2: Compilation of results of number of breaking waves with their respective time stamp relative to the start of the wave maker

#	H_S [m]	phase angle	Time [s]	breaker type
1	0.200	a	00:47	spilling
			00:52	whitecap.
			00:55	whitecap.
			01:15	spilling
			01:20	whitecap.
			01:23	whitecap.
7	0.225	a	00:47	spilling
			00:52	whitecap.
			01:15	spilling
			01:19	whitecap.
			01:23	whitecap.
8	0.250	a	00:48	spilling
			01:10	whitecap.
			01:15	spilling
3	0.200	b	00:55	whitecap.
			00:59	whitecap.
6	0.200	c	01:03	whitecap.

For direct comparison, the results in table 2 are sorted by phase angle distribution and then significant wave height H_S.
The following conclusions can be drawn: Firstly, for the same phase angle distribution, the number of breaking waves was observed to be constant, and the

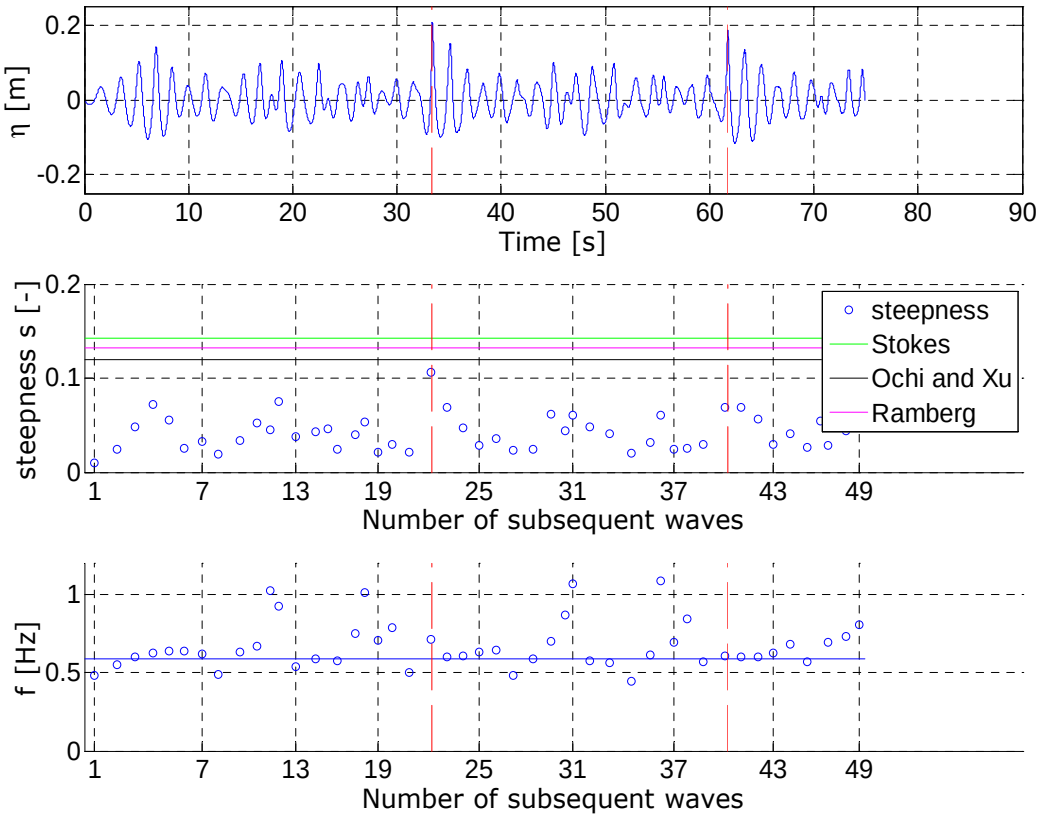

Figure 8: Time series of test 1 for wave gauge WG2 with H_S = 0.2 m and phase angle distribution "a". Position of wave-breaking is marked with dotted red lines. Top: water surface elevation η in [m]. Middle: wave steepness s = H/L for every wave with critical steepness thresholds of Stokes s_{cr} = 0.14 [13], Ochi s_{cr} = 0.19 [14], Xu s_{cr} = 0.19 [15] and Ramberg ε_{cr} = 0.21 [16]. Bottom: wave frequency f in [Hz] for every wave

wave-breaking occurs temporally and spatially at the same positions.

Secondly, an increasing significant wave height results in a decreasing number of whitecaps.

Thirdly, the randomness of the phase angle distribution and thereby, the randomness of the wave sequence in the time series, has a significant influence on the number of breaking waves; in contrast to phase angle distribution "a" with two spilling breakers, phase angle distributions "b" and "c" cause no breaking waves, only whitecapping. There might be two reasons for that: Either the time series were too short (approx. 50 waves) or an exemplary time series cannot represent all possible time series from one sea spectrum. Further test runs are indispensable.

Fourthly, even the second spilling breaker in a wave train is reproducible, which concludes that the first spilling breaker breaks always in the same way, though the breaking process is a highly non-linear and turbulent process.

In order to analyse the wave train modulation over time, the time series of wave gauge WG2 for test 1, and the steepness and frequency of every wave in the sequence, is given in Fig. 8.

The two spilling breakers occur at wave gauge WG2 at approx. 33 sec and 61 sec; their positions are marked with dotted red lines. For the first breaker, it can be observed that the steepness $s = H/L$ increases instantly at the moment of wave-breaking and the wave frequency f increases before breaking and drops afterwards, a behaviour also observed by Babanin et al. [12].

The second breaker does not show the same value s_{cr} and behaviour of the

steepness *s*. The reason is that the wave is already in the developed breaking process when reaching wave gauge WG2; the actual incipient breaker is not measured.
The critical steepness for the conducted model tests is $s_{cr} \approx 0.11$, which is smaller than the thresholds given in literature. Again, the reason is, that not the incipient breaker, but the breaker in progress, is measured.

Work in progress

The first set of test runs showed the following potential for optimisation in the test setup as well as in the test program. For a better detection of wave-breaking more wave gauges and video cameras are needed. For a better understanding of the influence of the random phase angle, test runs with a systematic relation of the phase angles will be conducted. Furthermore, test runs with variations of the remaining influencing factors, namely the peak periods T_P and water depths *d* will be carried out.

References

[1] Jonkman, J.; Butterfield, S.; Musial, W.; Scott, G.: Definition of a 5-MW Reference Wind Turbine for Offshore System Development. National Renewable Energy Laboratory: NREL/TP-500-38060, 2009.

[2] Jonkman, B.J.: TurbSim User's Guide: Version 1.50. National Renewable Energy Laboratory: NREL/TP-500-46198, 2009.

[3] Jonkman, J.M.; Buhl Jr., M.J.: FAST User's Guide. National Renewable Energy Laboratory: NREL/TP-500-38230, 2005.

[4] Ernst, B.; Seume, J.R.: Modelling Structural Uncertainty of Wind Turbine Rotor Blades for Aeroelastic Investigations. Seventh M.I.T. Conference on Computational Fluid and Solid Mechanics - Focus: Multiphysics & Multiscale, June 12-14, 2013, Massachusetts Institute of Technology, Cambridge, MA 02139 USA.

[5] Ernst, B.; Seume J.R.: Investigation of Structural Uncertainty of Wind Turbine Rotor Blades. 6. Dresdner Probabilistik-Workshop, 10.-11. Oktober 2013, Technische Universität Dresden.

[6] Ghanem, R.G.; Spanos, P.D.: Stochastic Finite Elements: A Spectral Approach. Springer-Verlag, New York, 1991.

[7] Bir G.S.: User‘s Guide to BModes (Software for Computing Rotating Beam Coupled Modes). NREL/TP-500-39133. Golden, Colorado, USA: National Renewable Energy Laboratory, 2005.

[8] Bir, G.; Jonkman, J.: Aeroelastic Instabilities of Large Offshore Wind Turbines Journal of Physics: Conference Series 75, 2007.

[9] International Electrotechnical Commission: IEC 61400-1: Wind turbines part 1: Design. 3rd edition, 2005.

[10] International Electrotechnical Commission: IEC 61400-3: Wind turbines part 3: Design Requirements for Offshore Wind Turbines. IEC, 1st edition, 2009.

[11] Ernst, B; Seume, J.R.: Investigation of Site-Specific Wind Field Parameters and Their Effect on Loads of Offshore Wind Turbines. Energies 2012, 5, 3835-3855, doi: 10.3390/en5103850.

[12] Babanin, A.; Chalikov, D.; Young, I.; Savelyev, I.: Predicting the breaking onset of surface water waves. Geophysical Research Letters, vol. 34, L07605, 2007.

[13] Stokes, G.G.: Supplement to a paper on the theory of oscillatory waves. Mathematical and Physical Papers, Volume I, Cambridge University Press, pp. 314-326, 1880.

[14] Ochi, M. K.; Tsai, C. H.: Prediction of occurence of breaking waves in deep water. Journal of Physical Oceano-graphy, American Meteorological Society, Volume 13, pp. 2008 – 2019, 1983.

[15] Xu, D.; Hwang, P. A.; Wu, J.: Breaking of wind-generated waves. Journal of Physical Oceano-graphy, American Meteorological Society, Volume 16, pp. 2172 – 2178, 1986.

[16] Ramberg, S. E.; Griffin, M.: Laboratory study of steep and breaking deep water waves. Journal of Waterway, Port, Coastal and Ocean Engineering, ASCE, Volume 113, 5, pp. 493 – 506, 1987.

2.3 Soil (WP 3)

Institute for Geotechnical Engineering
Martin Achmus, Kirill Schmoor

2.3.1 Motivation

By performing geotechnical design the most practical and popular way to take account for uncertainties in soil properties, loading or mechanical performance behavior is the application of partial safety factors for the resistance and the action. This approach is also known in the literature as the Load Resistance Factor Design (LRFD).

The Eurocode 0 (EC0) provides in appendix B first a scope on how reliability is treated in general within the Eurocodes. Also a classification of target reliabilities with respect to three different hazards classes, limit states as also two time periods were made. Appendix C summarizes in a short term the mathematical background on how partial safety factors can be calculated or calibrated for a specific problem.

According to the statement in EC0 most of the structures can be associated to the second hazard class (RC2) which entails moderate risk for human life. Therefore the prescribed partial safety factors should establish at least a reliability index of β = 3.8 within the LRFD for a return period of 50 years.

The aim of this work package is to validate the partial safety factors for mainly axially tension loaded offshore foundation piles in North Sea site conditions. Therefore a case study of a Reliability Based Design (RBD) for two common soil profiles and two design methods, the API-method and the ICP-method, is presented in detail. Moreover a calibration of partial safety factors was carried out to match the safety requirements of the EC0 more specifically. Also a more accurate determination of the required embedded pile length was achieved due to accounting more information within the design process like a model error.

2.3.2 Approach

Introduction

In this chapter first the applied methods and assumed conditions were presented. Thereby already some aspects were introduced in the PSB Annual Report 2012 [9]. To avoid repetition the reader will be referred to [9] at the corresponding points.

Design Methods

The tension bearing capacity of mainly axially loaded piles consists basically of the mobilized friction between the pile outer shaft area and the surrounding soil. Additionally if an open ended pile is used two different condition states “plugged” or “unplugged” have to be considered. In the unplugged case also the friction resistance between the inner pile shaft area and the inner soil can be taken into account. By assuming a plugged condition the effective weight of the inner soil plug can be added to the bearing capacity.

Generally it can be observed that in almost all design cases the tension limit state is the controlling one with regard to the required pile length. Therefore only tensile capacity is considered here. The pile resistance for the unplugged or plugged condition can be computed by applying Equation 1:

$$R_t = A_o \int f_t(z)\mathrm{d}z + \min[A_i \int f_t(z)\mathrm{d}z ; G'_p] \quad (1)$$

where:

A_o	Outer pile shaft area
$f_t(z)$	Skin friction for tension loading
A_i	Inner pile shaft area
G'_p	Effective weight of the inner soil plug

The ICP-method assumes a plugged condition for the determination of the tension pile resistance. Also no additional resistance by the inner soil plug is taken into account. The skin friction for non-cohesive soils according to the ICP-method can be determined by applying Equation 2. Therefore the trend of the skin friction is mainly influenced by the measured cone tip resistance.

$$f_t(z) = 0.016 q_c \left(\frac{\sigma'_v}{p_a}\right)^{0.1} A_r^{0.2} \left(\max\left[\frac{L-z}{D_o}; v\right]\right)^{-0.4} \tan\delta_{cv} \quad (2)$$

where:

q_c	Cone tip resistance
σ'_v	Overburden stress
p_a	Atmospheric pressure = 100 kPa
A_r	Effective area ratio $A_r = 1 - (D_i/D_o)^2$
D_i	Pile inner diameter
D_o	Pile outer diameter
L	Embedded pile length
v	Dimensionless parameter $v = 4(A_r)^{0.5}$
δ_{cv}	Interface friction angle.

The API-method differs between a “plugged” and “unplugged” resistance. For the tension limit state in almost all design cases the “plugged” resistance is design driving. The skin friction for the API-method basically derives from multiplication of the overburden stress and the β-factor, which depends on the soil density. For more detailed description on the calculation process of the API-method the reader is referred to [9], [2] and [3].

Pile System under consideration

For the performed study typical site conditions for the North Sea and typical ranges for the foundation pile properties were assumed.

Since the subsoil in the German North Sea mostly consists of dense sands with only limited intermediate cohesive layers, two idealized CPT profiles for homogeneous dense (Dr = 0.75) and very dense (Dr = 0.93) sands were considered. The effective unit weight was assumed to be 10 kN/m³, since this value represents a reasonable estimate for both soil densities.

The choice of pile properties depends on the type of foundation, the water depth and the subsoil condition at the desired location. In general it can be said that pile slenderness ratios (embedded length to diameter) between L/D = 10 and L/D = 40 are used. Thereby the pile outer diameter is varying between D = 1 m and D = 3 m, where the pile embedded length is commonly chosen to be between L = 20 m and L = 60 m. For the considered range of the load in this study a diameter of D = 2 m was chosen. The regular pile wall thickness which is commonly used can approximately be determined by t = D/40.

A characteristic load of V_k = 9 MN for a pile foundation with a supporting structure for a 5 MW windmill in the German North Sea with a water depth of 30 m was considered. Therefore typical 50-year extreme environmental values were assumed. Figure 1 shows the considered boundary conditions.

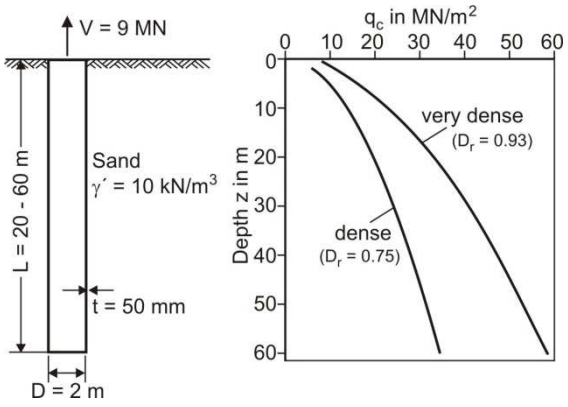

Figure 1: Considered pile system

Deterministic Design

The partial safety factors for the deterministic design of an offshore pile foundation in Germany are defined by the Eurocode 7 with the national supplementary code DIN 1054. Here a 50-year extreme event is studied. Thereby the corresponding partial safety factor for the load is defined as γ_L = 1.35. For the tension resistance of a pile a partial safety factor of γ_R = 1.5 according to DIN 1054 is applied. Together a product of partial safety factors - indicating the global factor of safety - of 2.03 is applied.

For the assumed CPT profiles with their corresponding relative densities the two introduced design methods were evaluated. Figure 2 shows the development of the characteristic resistance with increasing pile length. For very dense soil conditions a strong deviation between the methods must be noticed.

Table 1: Required deterministic pile lengths with corresponding reliability index

Design methods	D_r = 0.75		D_r = 0.93	
	API	ICP	API	ICP
Deterministic length	51.85	45.91	45.19	30.24
Reliability index	4.1	3.5	4.0	3.5

By assuming the characteristic load and partial safety factors a characteristic resistance of R_k = 18.23 MN is required to fulfill the deterministic design proof according to Equation 3. The corresponding pile lengths for the different methods and densities can be obtained from figure 2. Also table 1 summarizes the deterministically determined pile lengths.

$$V_k \gamma_L \gamma_R \leq R_k \tag{3}$$

where:

V_k Characteristic load
γ_L Partial safety factor for the loading
γ_R Partial safety factor for the resistance
R_k Characteristic resistance

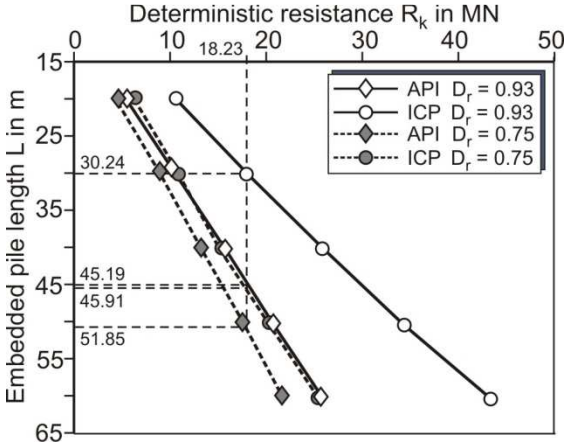

Figure 2: Resistances for the API and ICP method with increasing pile length

Subsoil modeling

The subsoil model basically consists of a 1-D autocorrelated random field of the cone tip resistance q_c.

The two assumed q_c profiles were applied as trend functions t_{qc} (z) where an inherent variability w_{qc} (z) as also an measurement error e_{qc} (z) were accounted. The corresponding random process of q_c(z) is calculated acc. to Equation 4:

$$q_c(z) = \left[t_{qc}(z) + w_{qc}(z)\right] \cdot e_{qc}(z) \tag{4}$$

Additionally also uncertainty in the unit weight as also a transformation error for the internal effective friction angle were applied. A more detailed description on the established subsoil model is given in [9].

Model error

A model error can be determined by comparing measured properties with calculated ones. In this way a model error is an indicator how reliable a calculation method is.

Jardine et al. (2005) obtained a model error for both methods where the following pile tests were considered: Closed-ended and open-ended piles, tension and compression test, steel and concrete piles and loose to very dense soil state.

Altogether 81 pile tests were evaluated. The statistical values are shown in table 2. Therein the model error is defined as the ratio of the measured to the calculated resistance.

Achmus & Müller (2010) compared measured with calculated results for the API and the ICP-method only with pile tests which are closely related to the boundary conditions in the North Sea. By this it can be seen how reliable these methods are to a special boundary sector.

Table 2: Model error (R_m / R_c) for the ICP-method and API-method

Method		Mean [-]	SD [-]	COV [-]
Jardine et al. (2005)	ICP-method, all pile tests	1.01	0.28	0.28
	API-method, all pile tests	1.15	0.58	0.50
Achmus & Müller (2010)	ICP-method, only related tests	1.16	0.19	0.16
	API-method, only related tests	1.26	0.14	0.11

Table 3: Stochastic parameters used for MCS

Basic variable	Notation	Mean	SD	COV	Distribution type
Unit weight	γ'	$10\ kN/m^3$	$1\ kN/m$	0.10	Normal
Inherent variability	w_{qc}	-	$6000\ kN/m^3$	$0.75 - 0.10$	Normal
Measurement error	e_{qc}	1	0.15	0.15	Normal
Transformation error φ'	$e_{\varphi'}$	0°	2.8°	0.07	Normal
Model error API	m_{API}	1.26	0.14	0.11	Normal
Model error ICP	M_{ICP}	1.16	0.19	0.16	Normal
Pile diameter	D	$2\ m$	-	-	Deterministic
Pile length	L	$20 - 60\ m$	-	-	Deterministic
Pile wall thickness	t	$0.05\ m$	-	-	Deterministic
Axial loading	V	5400	1890	0.35	Gumbel

In detail the following pile tests were considered: Open-ended piles, tension test, steel piles, dense to very dense soil state and slenderness ratios between 10 and 40.

By taking into account only pile tests within a range of 95% confidence interval, only 6 pile test for the ICP-method and only 4 pile tests for the API-method could be found. The mean and standard deviations for these related tests are summarized in table 2 and should be seen as rough approximations of the real values.

As it can be seen the overall model error for the ICP-method is smaller in mean and standard deviation compared to the overall model error for the API-method. By comparing the model error only for the related tests, it can be said that in average both methods underpredict the resistance. The standard deviation seems also to be smaller and also closer related to each other as in the overall case.

Stochastic variables and simulation

For each performed simulation with a certain pile length 6 million realizations within a plain Monte-Carlo simulation (MCS) were computed.

The inherent variability of the cone tip resistance w_{qc} was assumed to be constant with depth. By applying a standard deviation of 6 MN/m² the COV is varying between 0.75-0.20 for dense and 0.40-0.10 for very dense soil conditions. According to Phoon & Kulhawy (1999) the COVs were thereby in a typical range of 0.81 and 0.10. The vertical autocorrelation length for the cone tip resistance is indicated to be between 0.1 m and 2.2 m. Hence, the value of θ = 0.6 m was chosen for all simulations.

The buoyant unit weight γ', the measurement error for the cone tip resistance e_{qc} and the transformation error for the internal friction angle e_{φ} were modeled as uncorrelated and normally distributed random fields with typical values for the mean and standard deviation. The stochastic formulation for the load was chosen according the recommendation by Holicky et al. (2007) for a 50-year extreme environmental event.

All applied variables with their corresponding stochastic moments are summarized in table 3.

2.3.3 State of Work

Impact of Uncertainties

For the computed data sets first the COVs of the resistance distributions are evaluated. Additionally the corresponding parts which arise from the model error and soil uncertainties were estimated, as depicted in figure 3 for very dense soil condition.

For both methods the total variation of the resistance is much lower than of the load. For the API-method almost 11 % and for the ICP-method about 17 % were obtained. Further the model error is almost exclusively responsible for the variation of the resistance, especially for

the API-method. Also it can be noticed that the deviation arising from soil uncertainties is decreasing with embedded pile length, since an averaging effect becomes more dominant.

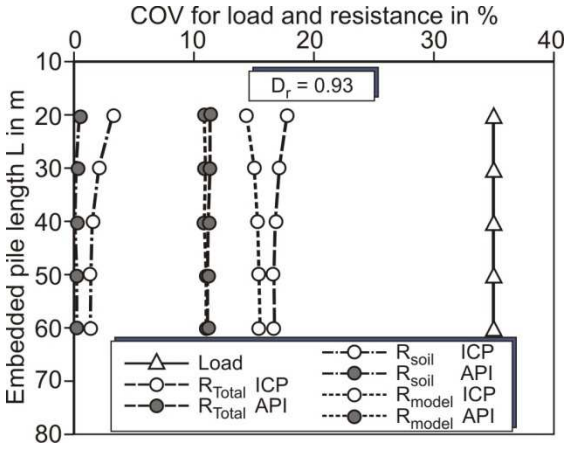

Figure 3: COV for the resistance and load with increasing pile length

Safety

The safety of a system can be described in terms of a reliability index β corresponding to Equation 5. In the following, β is also termed safety.

As already mentioned above the prescribed partial safety factors in the EC0 should establish at least a safety of β = 3.8 in a design system. However, offshore pile foundations for wind energy converters may also be associated to the third reliability class (RC3) which demands a safety of β = 3.3

$$\beta = \Theta^{-1}(1 - pf) \qquad (5)$$

where:

Θ	Cumulative standard distribution
pf	Failure probability

For the computed pile lengths the derived reliability index is shown in figure 4. Table 1 also presents the corresponding safeties for the deterministic required pile lengths.

Therefore it can be generally said that by applying the usual partial safety factors a safety of β = 3.5 according to the ICP-method and about β = 4.1 according to the API-method is achieved. Nevertheless, it should also be noticed that the API-method indeed yields a longer embedded pile length.

For a certain embedded pile length or safety it could be generally assumed that the real established safety or required pile length is between the computed values corresponding to these methods, respectively.

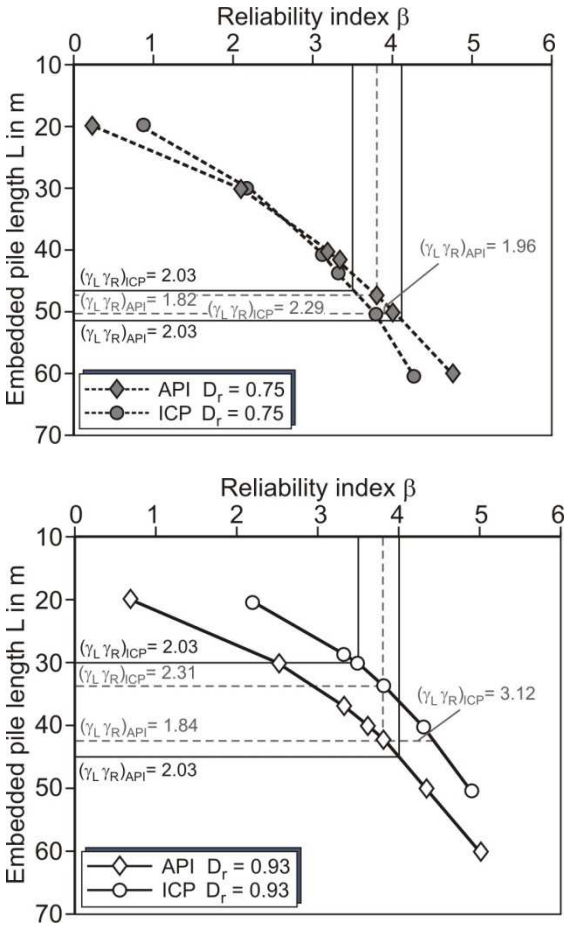

Figure 4: Evaluated safety with increasing pile length

Partial Safety Factors

Figure 5 elucidates the sensitivity values depending on safety. It can be seen that the sensitivity for the load is much higher than for the resistance. Generally the values are getting more uniform for higher reliability values and more dense soil conditions.

The corresponding partial safety factors which should be used for a given safety are shown in figure 6. For the API-method a resistance partial safety factor lower

Table 4: Product of partial safety factors for a safety according to the minimum of both methods

Design methods		$D_r = 0.75$		$D_r = 0.93$	
		API	ICP	API	ICP
$\gamma_L \gamma_R$	$\beta = 3.3$	1.59 (1.52)*	1.86	1.55	2.60 (1.87)*
	$\beta = 3.8$	1.96 (1.82)*	2.29	1.84	3.12 (2.31)*
* Corresponding partial safety factors product by not taking into account the minimum of both methods.					

than one was computed. This uncommon result is achieved due to applying model uncertainty in combination with nonuniform COVs. However, the product of both partial safety factors affects the safety within the deterministic design proof. In contrast both partial safety factors for the ICP-method are increasing continuously, where for very dense sand condition the partial safety factors tend to be more uniform, like also the sensitivity values.

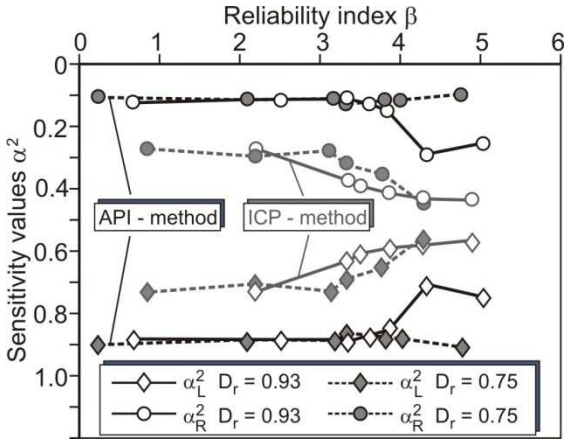

Figure 5: Load and resistance sensitivity values with increasing safety

Table 4 shows the products of partial safety factors which should be used within a deterministic design to achieve the given safeties according to the minimum of both methods. Comparing to the deterministic values, generally a decrease for the API-method and an increase for the ICP-method should be applied. Single partial safety factors as also the product can be estimated for a desired safety from figure 6.

Deterministic design vs. RBD

By performing reliability based design the same safety can be aspired as also more information, like a model error, can be taken into account. This leads to a more robust determination of the required pile length. Therefore table 5 summarizes the separation according to deterministic design and two reliability indexes. As it can be seen the gap between the obtained pile lengths via reliability based design is decreased about 61 % for dense and 41 % for very dense soil conditions.

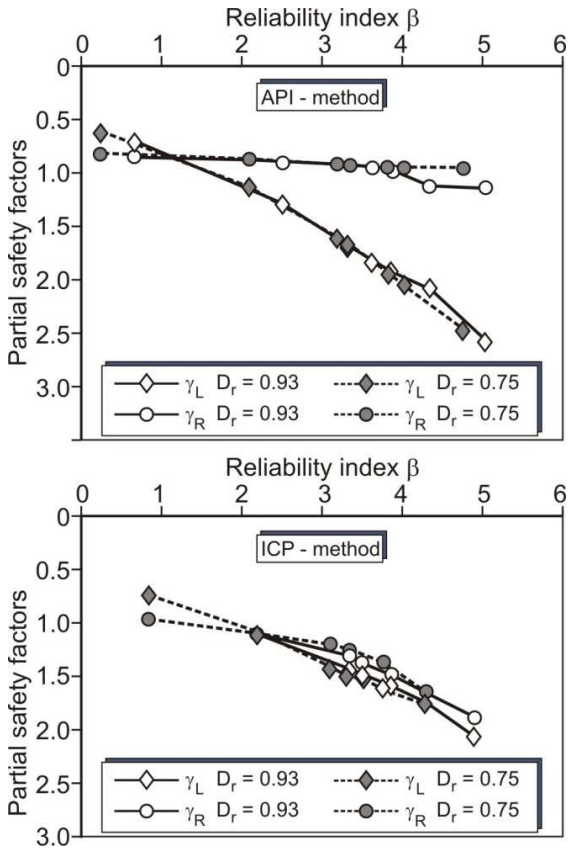

Figure 6: Partial safety factors required to achieve a certain safety

Conclusions

It could be determined that the use of partial safety factors according to DIN 1054 for mainly axially loaded foundation piles of offshore wind turbines leads in

Table 5: Comparison of the separation of required pile lengths for different designs

	ΔL (D_r = 0.75)	ΔL (D_r = 0.93)
For deterministic design	5.94	14.95
For reliability β = 3.3	1.46	8.61
For reliability β = 3.8	3.12	8.77

case of the API-method to a safety of β = 4.1, where in case of the ICP-method a safety of β = 3.5 was detected. Based on that, it generally can be assumed that the real safety is in the range of these values.
Also it was found that the variation for the resistance arises mainly from the model error and that the soil uncertainty is of much lower effect than it would be expected.
According to the computed results the partial safety factors should be decreased for the conservative API-method, where an increase for the ICP-method is recommended. This applies only for the considered systems.
A more specific determination of the pile length by applying reliability based design is possible, since more information is evaluated.

References

[1] Achmus, M. Müller, M.: Evaluation of pile capacity approaches with respect to piles for wind energy foundations in the North Sea, In S. Gourvenec, D. J. White (eds), Frontiers in Offshore Geotechnics Two, CRC Press: Balkema, 2010

[2] API: Recommended Practice for Planning, Designing and Constructing Fixed Offshore Platforms- Working Stress Design, API (RP2A-WSD); Dallas: American Petroleum Institut, 21st edition, 2006

[3] API Errata and Supplement 3: API Recommended Practice 2A-WSD, Recommended Practice for Planning, Designing, Constructing Fixed Offshore Platforms – Working Stress Design, 2007

[4] DIN 1054: Baugrund-Sicherheitsnachweise im Erd und Grundbau, Berlin: Deutsches Institut für Normung, 2010

[5] DIN EN 1990: Eurocode: Grundlagen der Tragwerksplanung; Berlin: Deutsches Institut für Normung, 2010-12

[6] Holicky, M., Markova, J. & Gulvanessian, H.: Code Calibration Allowing for Reliability Differentiation and Production Quality. In Kanda, Takada & Furuat (eds), Ap-plication of Statistics and Probability in Civil Engineering: Proceedings of the 10th International Conference. London: Taylor & Francis, 2007

[7] Jardine, R., Chow, F.C., Overy, R. & Standing, J.: ICP Design Methods for Driven Piles in Sands and Clays. London: Thomas Telford, 2005

[8] Phoon, K. K.; Kulhawy, F. H.: Characterization of geotechnical variability, Canadian Geotechnical Journal, 36, pp. 612-624, 1999a

[9] Probabilistic Safety Assessment of Offshore Wind Turbines, annual report 2012, Leibniz Universität Hannover, February 2013

2.4 Foundation and Support Structure (WP 4)

Institute for Steel Construction
Peter Schaumann, Sebastian Kelma

Institute of Structural Analysis
Raimund Rolfes, Jan Goretzka

Institute of Concrete Construction
Boso Schmidt, Michael Hansen

2.4.1 Motivation

Work Package 4 (WP 4) deals with design and optimization of support structures of offshore wind turbines (OWTs) with respect to probabilistic methods.
Loads acting on the turbine are transferred by the support structures of OWTs into the soil. Besides dead loads of the rotor nacelle assembly (RNA) and support structure, operation loads of the RNA as well as wind and wave induced loads have to be transferred to the soil.
The design of support structures shows small scatter with regards to material and geometry, as already stated in [1]. In contrast, loads from wind and waves as well as the load bearing capacity of the soil are afflicted with great uncertainties.
These uncertainties within design and optimization of support structures are considered by applying probabilistic methods and shall be investigated within WP 4.

2.4.2 Approach

Limit states which are the most critical for the structural design of OWTs were identified. One of the design-driving limit states is the maximum pile resistance for tension loading. The objective was to find the ultimate limit state function for the pile resistance for tension loading in cooperation with WP 3 (soil).
To verify the ultimate limit state for the structural design, the extreme response of the OWT during a storm has to be analysed. According to valid standards such as [2], a 50-year storm has to be considered for the structural design. Here, the design load case (DLC) 6.1 deals with the extreme response of the idling OWT. Different methods for the calculation are stated, with the following parameters:

- DLC 6.1a: full dynamic simulation for combination of extreme sea state and extreme wind speed
- DLC 6.1b: extreme steady wind speed and reduced wave height
- DLC 6.1c: extreme deterministic wave height and reduced steady wind speed

DLC 6.1c is applied during ongoing research. Even though the full dynamic simulation of the OWT as defined in DLC 6.1a might reflect reality better, a few disadvantages exist. At least 50 full dynamic simulations are required for each combination of wind speed and sea state, which requires high numerical effort and therefore is very time-consuming. Also, the non-linearity of the wave kinematics has to be considered, especially for high waves that occur during a storm. For simulations the sea state is usually represented as sum of many wavelets with linear wave kinematics. Models exist to represent the nonlinear wave kinematics of sea states, but they were not applied yet.
Within standards, usually a probability of failure is defined that is permitted for OWTs. For example, the probability of failure is set to 10^{-4} in [3]. Therefore, an idling OWT during an 1-year storm is investigated, in contrary to a 50-years storm as recommended in [2].
While applying DLC 6.1c for an 1-year storm, scattering parameters to describe the wind and the sea state are taken into account for a probabilistic approach. The probability distributions of 1-year extreme wind speed and significant wave height are based on environmental data from the FINO1 measuring platform. Eventually, parameters of the sea state have to be adjusted to the actual site (cf. [4], [5]).
Steady wind- and wave-induced loads acting on the OWT are determined separately and independently of each

other, by applying the software Flex5 and Poseidon [6], respectively.
By using the Monte-Carlo simulation, the probability of failure can be determined for scattering parameters for soil (cf. WP 3, [5]), wind and sea state. In cooperation with WP 3, scattering of soil parameters is taken into account (cf. [5], [7]).
For an advanced probabilistic design, the dependence of the input parameters also is to be considered.
Besides the ultimate limit state for the pile resistance for tension loading, fatigue also has to be considered during the design process. Especially branched structures such as joints of jackets and tripods are critical. In order to find a more accurate design, time series of loads acting on joints of a jacket structure generated by numerical simulations will be evaluated concerning fatigue damage by using adequate probabilistic approaches.

2.4.3 State of Work

Modelling

The model of the investigated OWT consists of the NREL 5-MW Turbine [8], which was used within the OC3 project [9], and jacket substructure as defined within the OC4 project [10]. For a more detailed description of the OWT model, confer to [5]. The OWT is connected to the seabed by foundation piles, whose dimensions are given in [10].
As a simplification of the modelling, the piles were not modelled for the numerical investigations. Instead, different boundary conditions to describe the interaction between OWT and soil are investigated (figure 1). At one hand, the bearing of the OWT to the seabed was modelled as hinged (figure 1 (b)). Using this approach, the absolute values of forces are maximal compared to other boundary conditions, since the energy that is transferred into the seabed only leads to forces, but no bending or torsional moments at the hinged connection. In contrast, minimum absolute values of forces are obtained for clamped bearings (figure 1 (c)). Here, the same amount of energy leads to forces and additionally bending and torsional moments and hence to reduced forces compared to a hinged bearing.

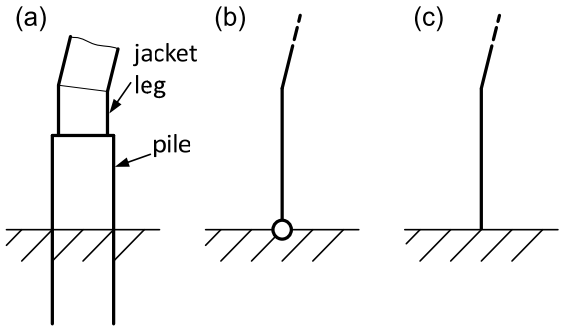

Figure 1: (a) Foundation in soil, (b) modelled as a hinged bearing, (c) modelled as a clamped bearing

The realistic values for the axial forces at the pile's head lie within the range of the values which are determined by using clamped and hinged bearings.
In order to determine more accurate values for the reaction forces, a more detailed model of the soil and its non-linear behaviour shall be applied. For example, a system of springs and dampers can be implemented as recommended by API [11].Different boundary conditions of the connection between OWT and soil also affect the Eigen-frequencies of the OWT and hence affect the calculation of the fatigue damage.

Wind-induced loads

For DLC 6.1c, an idling OWT is loaded by a wind field with wind shear and without turbulence. Hence, the dynamic response of the OWT is negligibly small.
In order to find the steady wind-induced loads, time series of wind-induced axial loads acting on the foundation piles were generated using the previously mentioned wind field. Here, each wind speed at hub has to be considered that is covered by extreme value distribution of wind speeds for an 1-year storm. Flex5-Poseidon coupling was used for the determination of the steady wind-induced loads.

Similar to the function to calculate the wave-induced loads in dependence of the significant wave height [5], a function is found to calculate the steady wind-induced loads F_{wind} (in kN) acting on the foundation piles in dependence of the wind speed v (in ms^{-1}). Equations (1) and (2) are found for hinged (index *h*) and clamped bearings (index *c*), respectively,

$$F_{h,wind} = 1.682 \cdot v^2 - 14.551 \cdot v + 245.786. \quad (1)$$

$$F_{c,wind} = 1.415 \cdot v^2 - 0.169 \cdot v + 1.557. \quad (2)$$

In figure 2, the steady wind-induced loads in dependence of the wind speed are plotted, with the red line for hinged bearings and the blue line for clamped bearings.

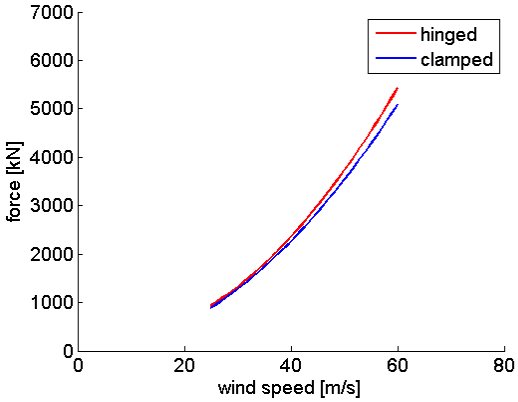

Figure 2: Wind-induced loads in dependence of the wind speed with (red) hinged bearings and (blue) clamped bearings

As already mentioned, one can see that the axial wind-induced loads acting on the foundation piles are reduced for clamped bearings in comparison to hinged bearings. For example, the wind-induced load is reduced by about 4.0 % for the mean wind speed $v_{w,mean}$ = 31.368 ms^{-1}. For full dynamic simulations as required for DLC 6.1a [2], turbulence of wind fields as well as the resulting scattering of dynamic response has to be considered. Here, an extreme-value distribution of the wind-induced loads also can be found. An investigation of extreme wind-induced loads acting on foundation piles was carried out in [12], but only for one wind speed. Combining this distribution with the distribution of the extreme wind speed occurring during an 1-year storm, a joint distribution is given,

$$p(v,F) = \int_v \int_F p(F|v)p(v)\,dFdv. \quad (3)$$

Due to the high numerical effort, it is not reasonable to determine the distribution $p(F|v)$ of extreme wind-induced loads for each wind speed to be considered. However, a method was proposed to reduce the number of required simulations. First, the extreme-value distribution of wind-induced loads is found for one wind speed as carried out in [12]. Second, the parameters describing the distribution are normalised by mean value and standard deviation of the investigated wind speed, which are almost constant for each time series. On basis of these normalised parameters, the extreme-value distributions of wind-induced loads can be found for other wind speeds.
More details can be found in [13].

Wave-induced loads

In annual report 2012 the influence of water depth on significant wave height was estimated by using equations of the Shore Protection Manual [14]. According to these equations, water depth and fetch length have a very large impact on the significant wave height.
Significant wave heights in different water depths were evaluated at three sites in the German Bight to verify this very rough and location-independent estimation. In addition to the measured values at FINO 1, data of FINO 3 and North-Sea-Buoy II (NSB 2) were evaluated. The methods for data analysis have been already discussed in recent annual reports. Actually, the results are focused.

FINO 3 was built 2009 in a water depth of 22 m about 80 km in the north-west of Sylt. NSB 2 is located 150 km in the west of Sylt in 42 m water depth. The evaluation of FINO 1 and NSB 2 measurement data are based on a seven-year measurement period. For the evaluation of FINO 3 data only a four year measurement period could be used. Therefore, these results are less reliable.

The probability density functions of one week extreme values of H_S are shown for each site in figure 3.

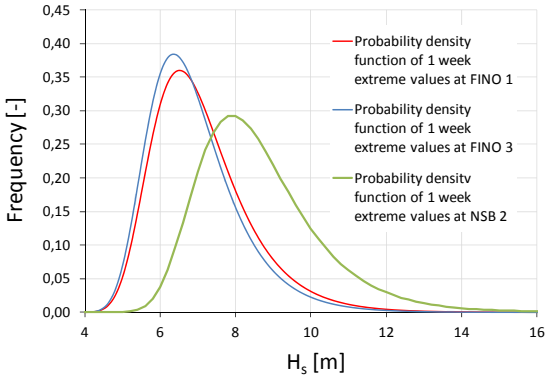

Figure 3: Probability density function of one week extreme values at three different measurement sites in the German bight

The extreme values of each measurement site can be well approximated by a Gumbel distribution. Both, mean values and standard deviation of H_S, increases with deeper water. The comparison of the statistical values is shown in table 1.

Table 1: Statistical values (mean m_{Ext} and standard deviation σ_{Ext}) of the one-year extreme value distribution of H_S at the site of FINO 1, FINO 3 and NSB 2

water depth	parameter	distribution	m_{Ext} [m]	σ_{Ext} [m]
22	H_S	Gumbel	6.893	1.227
30	H_S	Gumbel	7.091	1.311
42	H_S	Gumbel	8.633	1.611

Based on these data the statistical values of H_S in 50 m water depth are approximated. Assuming a linear relationship a mean value of the significant wave height of 9.22 m can be expected in 50 m water depth. This corresponds to a 30 % higher mean significant wave height with an increase of water depth of 30 to 50 m. The standard deviation of H_S increases in the same way as the mean value, i.e. the coefficient of variation is nearly constant over the water depth, c.f. figure 4.

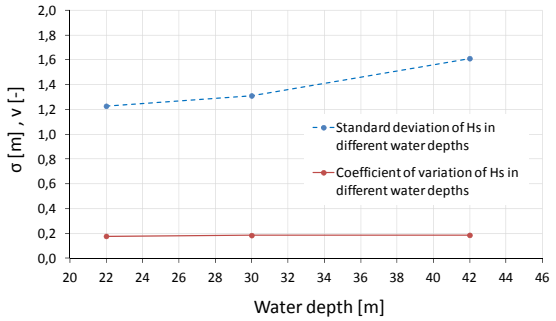

Figure 4: Standard deviation and coefficient of variation of H_s in different water depths

In addition to scattering loads the correlation between load parameters has a substantial influence on the reliability of the whole OWT. For fatigue load simulations and structural analysis of various operating states conditional input parameter are taken from so called scatter diagrams, cf. [15]. The correlation of different environmental parameters for frequently occurring events is considered in this way.

For extreme events with return period of 50 or 100 years there are no measurement data available. According common regulations, for example [2], these extreme single events should be modelled conservatively unless a joint probability distribution exists. In the past there was often a lack of adequate data bases to determine joint probability distributions.

Synchronously measured series of wind speed, wind direction, wave heights, wave periods and wave directions for a long measurement time are available with the FINO 1 measurement data. Based on a temporal assignment of these data, first investigations of simultaneously occurring

extreme wind speed and significant wave heights have been done. The investigations show that extreme wind events do not coincide with the extreme sea conditions. For both, extreme wind speed and significant wave height, also direction dependencies could be detected, cf. figure 5 and 6.

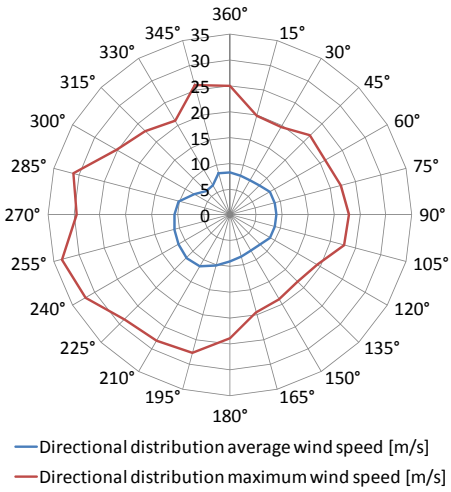

Figure 5: Directional distribution of average and maximum wind speed at the FINO 1 platform

The highest average and maximum wind speed is expected from the direction west-south-west.

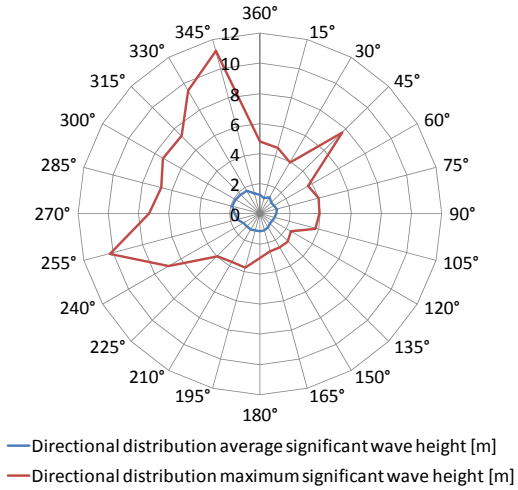

Figure 6: Directional distribution of average and maximum significant wave height at the FINO 1 platform

The direction of the maximum significant wave height is offset by almost 90 degrees. The maximum significant wave height is expected from north-north-west. A simultaneous occurrence of extreme wind speeds and significant wave heights with a direction offset of 90° can be excluded by the measurement data. These preliminary studies demonstrate that a simple superposition of rectified extreme wind speeds and sea states is unrealistic and leads to inefficient design results.

Failure mode analysis of ultimate bearing capacity for axially loaded piles

The maximum pile resistance as well as pile forces for tension loading of a jacket support structure were carried out. The structure was adapted to fulfil the environmental conditions at the site of the FINO1 measuring platform (c.f. [5]).

Two different kinds of bearing were investigated. In a first analysis the model of the jacket support structure is hinged at the seabed, whereas in a second study the piles are clamped at the seabed. The failure mode of pile heaving is indicated by the probability of failure P_f. In order to calculate the extreme response of the wind turbine, transfer functions of the maximum wave and wind induced pile tension forces were ascertained based on statistical data of a one-year storm. These functions are compared to the maximum pile resistance within the limit state function

$$F_{wave} + F_{wind} < F_{soil} \tag{4}$$

Therein, the maximum pile loads (in kN) depending on significant wave height H_s (in m) and wind speed v_w (in m/s) respectively, are calculated using the functions

$$F_{h,wave}(H_s) = 13.4 \cdot H_s^3 - 95.2 \cdot H_s^2 + 711.8 \cdot H_s - 317.5 \tag{5}$$

$$F_{h,wind}(v) = 1.682 \cdot v^2 - 14.551 \cdot v + 245.786. \tag{6}$$

in case of a hinged bearing at the seabed (c.f. [5]). In case of a clamped bearing the following functions were derived,

$$F_{c,wave}(H_s) = 11.8 \cdot H_s^3 - 85.0 \cdot H_s^2 + 613.7 \cdot H_s - 273.9 \quad (7)$$

$$F_{c,wind}(v) = 1.415 \cdot v^2 - 0.169 \cdot v + 1.557. \quad (8)$$

These loads acting on the OWT are determined separately and independently of each other, as it is proposed in [12].
The ultimate limit state function of pile resistance for tension loading was carried out in cooperation with WP 3 (soil). The axial pile resistance is modelled as a single random variable $R_{p,ax}$ (in kN), c.f. [5]. Plugged piles are assumed and a dense sand layer is considered with $D_r = 0.75$. The pile length is set to 45m. Within these calculations of the soil resistance, a model error R_{err} is taken into account as described in [7] and multiplied to the axial pile resistance. Furthermore, a dead weight of the four foundation piles at about 538 t is added to the right hand side of eq. (4).
The probability of failure is determined from eq. (4) for $N = 10^6$ designs generated by Monte-Carlo method using the statistical values shown in table 2.
Resulting distributions of the maximum pile tension resistance and forces acting on the model with a hinged bearing are plotted in figure 7. The probability of failure is calculated to $P_f = 6.0 \cdot 10^{-4}$.

Table 2: Statistical values used for the failure probability calculation.

parameter	distribution	mean value	STD
H_S [m]	Gumbel	7.091	1.311
v_w [m/s]	Gumbel	31.368	4.123
$R_{p,ax}$ [kN]	Normal	15845	269
R_{err} [-]	Normal	1.26	0.14

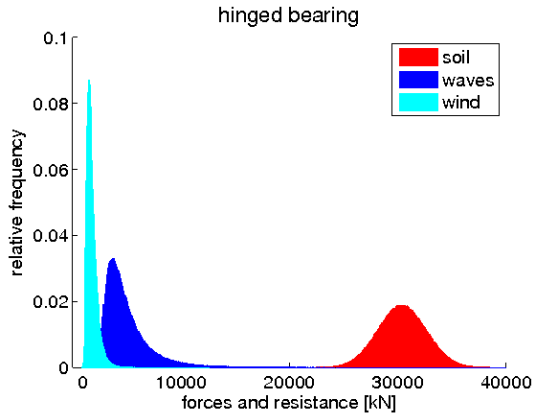

Figure 7: Resulting frequency distributions of forces and resistance within the failure probability calculation for the model with hinged bearing

In the case of a clamped modelled bearing, resulting distributions of the maximum pile tension resistance and forces are plotted in figure 8. The probability of failure is determined to $P_f = 3.0 \cdot 10^{-4}$.

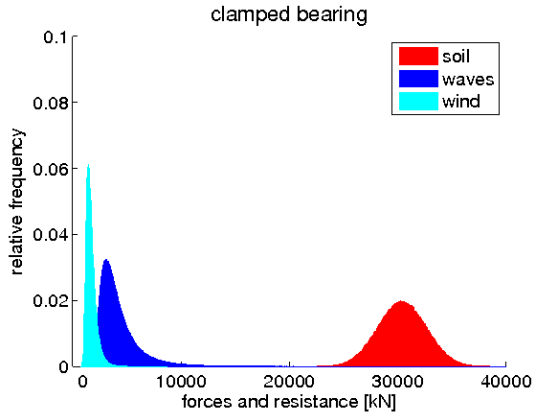

Figure 8: Resulting frequency distributions of forces and resistance within the failure probability calculation for the model with clamped bearing

As can be seen in figure 7 and 8, wave induced forces play the crucial role in this failure mode because of its high standard deviation.
Compared to the target probability of failure of 10^{-4} as set in [3], the determined probability of failure still is too high. By using a more advanced probabilistic model such as a joint distribution of wind speed

and significant wave height, the probability of failure might be reduced.

Probabilistic Fatigue Design of Jacket Joints

Besides the ultimate limit state, fatigue has to be considered for the structural design of OWTs. During their life-time, OWTs and especially branched structures such as jackets and tripods are stressed by fatigue loads caused by wind, operation and sea state. Joints are highly stressed due to their geometry.

In valid standards such as [2], design load cases to calculate the resulting fatigue damage of OWTs during power production are defined in DLC 1.2. Here, six numerical simulations of the OWEC with a duration of ten minutes and different wind seeds and sea states are required for each wind speed, that has to be taken into account.

The duration of the simulated time series are too short for probabilistic evaluation, especially for the occurrence probability of high stress ranges. It is assumed that especially very high stresses occurring with a very low percentage are decisive for the fatigue design. It is reasonable to estimate the distribution of the very high stresses by applying the peak-over-threshold method. A minimum duration of 30 minutes is proposed in [16]. Also, a high number of simulation are necessary to estimate the distribution of the very high stresses accurately.

Eventually, many simulations in time-domain are required to estimate the distribution of the stress ranges $\Delta\sigma$ and its tail of very high stress ranges.

Usually, the fatigue damage will be calculated by the Palmgren-Miner rule,

$$D = \sum_i \frac{n_i}{N_i}, \qquad (9)$$

where n_i is the number of cycles associated with the stress range and $\mathrm{N_i}$ is the endurance (in cycles) for a stress range $\Delta\sigma_\mathrm{i}$. For the probabilistic design, the distribution of stress ranges is applied for the calculation of the fatigue damage.

Instead of using many time series for the evaluation of the fatigue damage, it is reasonable to find a spectrum of the stresses in frequency domain on basis of only a few simulations in time-domain. On basis of the found solution in frequency-domain, time-series can be generated with considerably less computational effort, which can be evaluated concerning their distribution function.

Further investigations about the applicability of the frequency-domain have to be carried out.

2.4.4 Summary and Outlook

During the reporting period, the topics of research were the probabilistic evaluation of the ultimate bearing capacity for axially loaded piles as well as a more advanced evaluation of environmental data for the considered site.

Further development in probabilistic analysis of the ultimate bearing capacity for axially loaded piles was conducted. Monte Carlo simulations were carried out in order to determine the probability of failure. In corporation with WP 3, an adequate model was applied to describe the scattering of the soil behaviour. Steady wind- and wave-induced loads were calculated on basis of environmental data by using previously determined equations. Scattering of the environmental data is considered by using the extreme-value distribution for an 1-year storm, while no joint distributions between the data were taken into account.

Different axial loads acting on the pile head occur in dependence of the boundary conditions which are applied to describe the behaviour of the soil. Until now, the soil-pile interaction only was modelled as hinged or clamped bearings. By using a more detailed model of the soil, more realistic loads can be determined, which also leads to a more realistic probabilistic design of the piles.

In the next step, the ultimate limit state function of the bearing capacity for axially loaded piles shall be finalized. Besides the probabilistic approach to determine the ultimate bearing capacity for axially loaded piles, the investigation of the fatigue limit state shall be pursued, using adequate stochastic tools.

References

[1] Probabilistic Safety Assessment of Offshore Wind Turbines. Annual report 2010, Leibniz Universität Hannover, February 2011.

[2] IEC 61400-3: Wind turbines - Part 3: Design requirements for offshore wind turbines. Genf, January 2010.

[3] Det Norske Veritas: DNV-OS-J101, Design of Offshore Wind Turbine Structures, Det Norske Veritas (DNV), Høvik, Norway. October 2010.

[4] Probabilistic Safety Assessment of Offshore Wind Turbines. Annual report 2011, Leibniz Universität Hannover, February 2012.

[5] Probabilistic Safety Assessment of Offshore Wind Turbines. Annual report 2012, Leibniz Universität Hannover, February 2013.

[6] Böker, C.: Load simulation and local dynamics of support structures for offshore wind turbines. Dissertation, Leibniz Universität Hannover, 2009.

[7] Schmoor, K.A.; Achmus, M.: On the validation of reliability and partial safety factors for axially loaded piles in dense sand. 4th International Symposium on Geotechnical Safety and Risk (4th ISGSR), Hong Kong.

[8] Jonkman, J.; Butterfield, S.; Musial, W. and Scott, G.: Definition of a 5-MW Reference Wind Turbine for Offshore System Development. NREL/TP-500-38060. NREL: Golden, CO, 2009.

[9] Jonkman, J.; Musial, W.: IEA Wind Task 23 Offshore Wind Technology and Deployment – Subtask 2 The Offshore Code Comparison Collaboration (OC3) – Final Report. NREL: Golden, CO, 2010.

[10] Vorpahl, F.; Popko, W.; Kaufer, D.; Description of a basic model of the "Upwind reference jacket" for code comparison in the OC4 project under IEA Wind Annex XXX. Technical Report, Fraunhofer Institute for Wind Energy and Wind System Technology (IWES), 2011.

[11] American Petroleum Institute: Recommended Practice for Planning, Designing and Constructing Fixed Offshore Platform – Working Stress Design. API (RP2A-WSD), 21st edition, Dallas, 2007.

[12] Seidel, M.; Kelma, S.: Stochastic modelling of wind and wave induced loads on jacket piles. Stahlbau, vol. 81, issue 9, pp. 705-710, Ernst&Sohn, Berlin, 2012.

[13] Schaumann, P.; Kelma, S.: Probabilistic Design of Extreme Loads Acting on the Foundation Piles of a Jacket during an 1-Year Storm. Proceedings of 9th PhD Seminar on Wind Energy in Europe, Uppsala University Campus Gotland, 2013.

[14] Coastal Engineering Research Center: Shore Protection Manual. Washington, 1984.

[15] Bericht Nr. 1149 Teil 5: Stand der Forschung zur Korrelation und Richtungsabhängigkeit von Wind und Welle. Interner Bericht, Institut für Massivbau, Leibniz Universität Hannover, November 2013.

[16] Chen, P.W.: A Reliability Based Design Methodology for Extreme Responses of Offshore Wind Turbines. Dissertation, DUWIND Delft University, 2002.

2.5 In-Situ Assembly (WP 5)

Institute of Building Materials Science
Ludger Lohaus, Michael Werner

2.5.1 Motivation

Support structures and turbines of offshore wind turbines are prefabricated segmentally onshore, which offers the possibility of a high level quality control. Contrary to this, the connections between the piles and the substructure are manufactured under harsh offshore conditions. The gap between pile and sleeve, the so-called grouted joint, is filled with a high-performance mortar called “grout”. These grouted joint connections are commonly used in almost all kinds of offshore structures.
The main problem during the installation process is the grouting procedure under offshore conditions [1]. Due to the inaccessibility of the execution site, it is difficult to establish an effective quality control to ensure the correct *in situ* assembly of grouted-joint connections.

2.5.2 Approach

In this work package “supporting structure production *in situ*”, the risk factors of the grouted joints during the execution process will be evaluated, focusing on the material behaviour of the grout. Furthermore, concepts used for monitoring and minimising possible defects during execution will also be developed.
The work package is divided into six parts:

i) analysis of common supporting structure;
ii) types and the positions of grouted joints;
iii) analysis of boundary conditions;
iv) Preliminary Hazard Analysis (PHA) of the *in situ* assembly process;
v) Fault Tree Analysis (FTA); and
vi) experimental investigations.

The findings of the PHA and the FTA will be used to develop concepts to minimise possible defects, to ensure quality control and devise management solutions.
The flow behaviour and the material properties of fresh grout inside the gap between the pile and the sleeve can not be observed and have been unknown until now [2]. And therefore is important to estimate the effect of possible defects during the application process. Therefore, a special formwork with a transparent front panel has been constructed to observe the phenomena that occur during and after the grouting process. Exemplary failure modes will be simulated in this formwork to obtain basic knowledge of the whole situation.

2.5.3 State of Work

The analysis of the supporting structures shows different kinds of grouted joints and their exposure to seawater [3]. An effect of water in the annular gap of the grouted joints on the flow behaviour and the compressive strength is supposable. The laboratory testing facility was developed for grouting tests with and without water in the annular gap. The first grouting test without water showed minor or no negative effects on the compressive strength of the hardened grout.
Further tests [4] showed the influence of water which was preliminary filled into the grout gap over a height of 20 cm. The result was a reduction of up to 15% of the compressive strength of the grout in the main part of the test specimen and up to 70% in the upper parts (10 cm). This was mainly based on an intermix with the grout material, the lubrication mix and the water [4].
The PHA shows critical conditions, possible failures and their effects which can occur during a grouting procedure. Some of these failure modes were simulated with the laboratory testing facility to investigate possible phenomena and their influence on the compressive strength of the grout material.

Simulation of possible failure modes

Three scenarios were simulated based on the findings of the PHA:

i) a critical condition induced by extended pumping times;
ii) possible failure modes induced by a blocked grout line; and
iii) a procedure for limitation of defects induced by a permanently blocked grout line.

Therefore, a partly filled test wall was filled up from the top with a stinger by using the contractor method [5]. This method is used for the underwater casting of concrete. This method is well-known as “grouting with a stinger” in the offshore oil and gas industry [1]. Furthermore, effects of water-filled grout gaps and effects occurring by using a lubrication mix were analysed within the five tests. A small amount of material flows as overflow out of the top of the formwork in each test.

The first test simulated a breakdown of one of two mixers for the grout supply. For this simulation, the lowest pumping speed was chosen (approximately 0.11 m^3/h), the formwork was filled up to 20 cm with water and no lubrication mix was used. A grout with a low water content was used. With this set-up, effects of a low pumping speed and the influence of the lubrication mix were observed.

The following two tests simulated blocked grout lines. A lubrication mix was used in both tests and the gap in the formworks was filled with 20 cm of water. The formwork was filled with grout up to half of the height. Test 2 simulated a directly attached grout hose to the grouted joint so that a flushing of the grout line was possible after the break. Fresh grout was used to fill the formwork to the top from the inlet after 2.5 h. Test 3 simulated a grouted joint with fixed grout lines on the supporting structure. Because of this, a flushing of the grout lines is not possible. The material in the lines and in the pump was used after a break of 3.5 h. In both cases, a grout with a low water content was used.

Tests 4 and 5 simulated a half-filled grouted joint and permanently blocked grout lines. Test 4 was conducted with a grout with a high water content and with a 20 cm water-filled grout gap. A lubrication mix was used. The formwork was filled up to 80 cm with grout and then the filling process was stopped for 165 min. This should simulate the time taken to connect new grout lines and to insert the stinger from the top of the grouted joint into the grouted joint. The grout lines and the stinger were flushed by a lubrication mix until sound grout left the stinger. No additional lubrication mix was pumped into the formwork. Test 5 was for the evaluation of Test 4. Therefore, the formwork was filled with a grout with a high water content. The gap in the formwork was not filled with water and no lubrication mix entered the formwork. The following filling procedure was similar to Test 4. Test 5 could be seen as an optimum for this method because of less disturbance of the grout material.

Test results

After a period of hardening for the grout, sawed and grinded samples of the wall were taken at several positions to evaluate the compressive strength distribution of the grout. Approximately 2 cm of weak grout from the top and the bottom were cut of. The results were compared with test samples, according to [6]. A set of three grout samples with the dimensions 40 mm x 40 mm x 160 mm for each test were used for the comparison of the compressive strength. Figures 1 to 5 show pictures of the surfaces of the test walls on the left side. An interpolated map of the relative compressive strength compared with the reference test samples is shown on the right side. The values on this map give the location and the value of the relative compressive strength which was used for the interpolation.

Test 1 shows that the compressive strength is almost equal to the reference in most of the areas. A decrease up to 13 percent was detected in the upper left and right area. The fresh material seems to flow mainly from the middle part of the formwork up to the top. Hardly any intermix between the grout and the water could be observed. Figure 1 shows the results of Test 1.

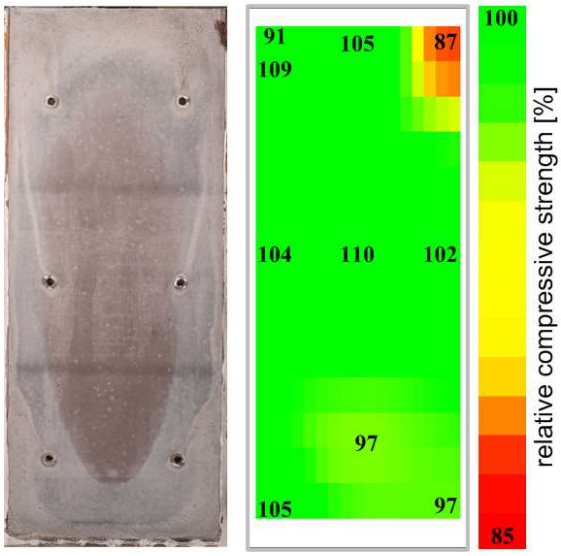

Figure 1: Test 1: low pumping speed, without lubrication mix, 20 cm water

The results of Test 2 are shown in figure 2.

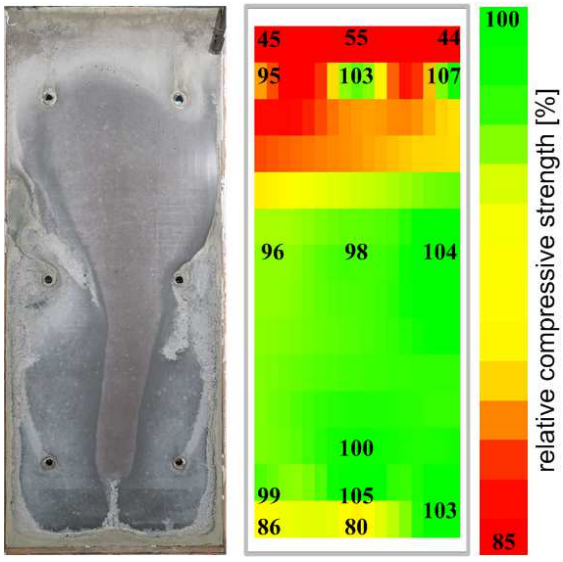

Figure 2: Test 2: blocked line for 2.5 h, lubrication mix, 20 cm water

Equal compressive strength regarding the reference grout samples were observed in the middle part of the wall. In the upper part, reductions up to 56 percent of the compressive strength were detected. Reductions up to 20 percent were noticed in minor parts at the bottom of the wall. An intermix between the lubrication mix, the water and the grout could be observed at the bottom, but mainly in the upper parts. The fresh grout material which was pumped in after the blockade should flow in a small channel in the middle of the formwork up to the top. The layer of intermixed grout material in the middle of the wall was delivered partly to the top.

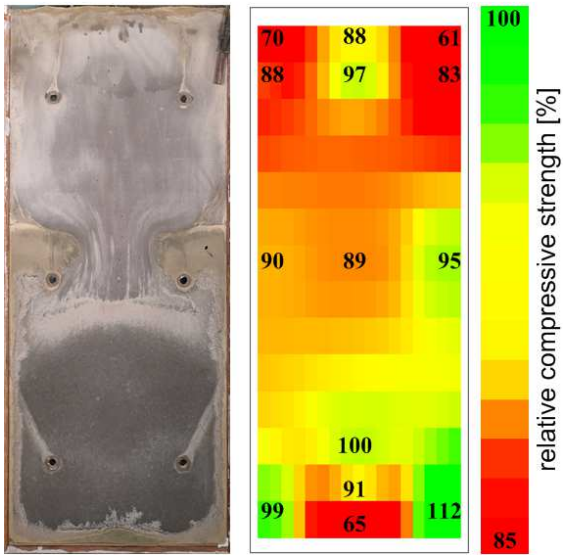

Figure 3: Test 3: blocked line with grout inside for 3.5 h, lubrication mix, 20 cm water

Test 3 shows a reduction of the compressive strength close to the whole area of the test wall (figure 3): in the middle part, up to 11 percent, in the upper part, up to 39 percent, and in the lower, up to 35 percent close to the inlet. An intermix between the grout, the lubrication mix and the water was primary noticed before the first stop of the filling process. The intermixed material in the middle of the wall was only delivered partly to the top of the formwork.

Test 4 shows reductions up to 59 percent in the upper and the lower parts of the testwall. Reductions in the upper middle part were detected to about 20 percent, and partly up to 36 percent. Equal values for the compressive strength were found in the lower middle part of the walls. An intermix between the materials could be seen over approximately two-thirds of the wall.

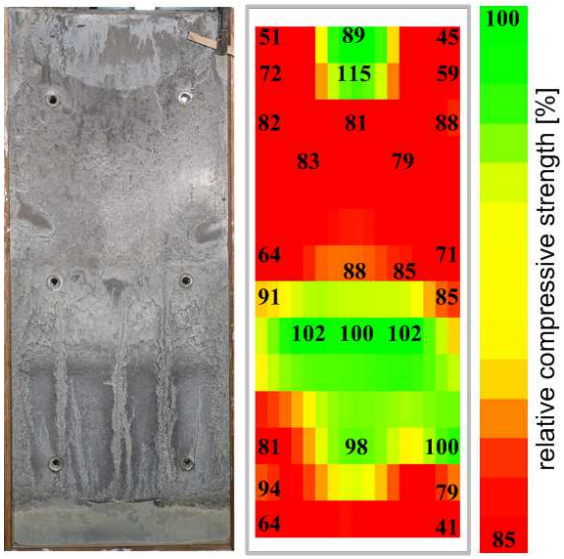

Figure 4: Test 4: Blocked lines, stinger, lubrication mix, 20 cm water

The results of Test 5 are shown in figure 5. This test shows that the compressive strength is almost equal to the reference values in most of the areas. Reductions of the compressive strength up to 16 percent were noticed fractionally in the upper and lower area of the wall. Because of the absence of water, no intermix of grout material occurred.

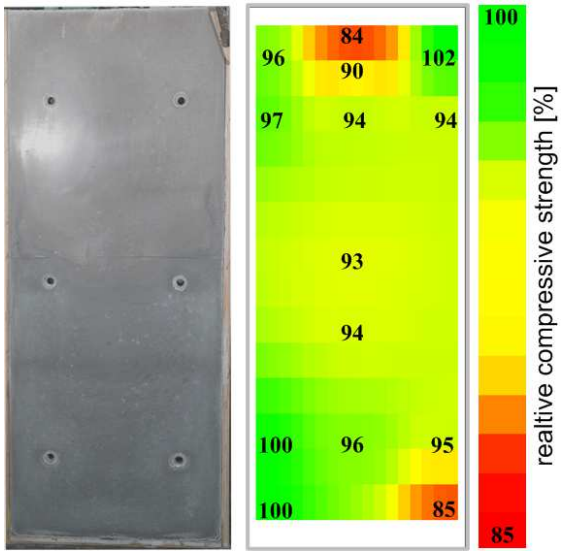

Figure 5: Test 5: Blocked lines, stinger, without lubrication mix, without water

Conclusion of the failure modes

Test 1 shows that a slow pumping speed has no negative influence on the compressive strength when the initial setting time of the grout is not reached.

Tests 2 and 3 show a minor negative influence on the compressive strength when a line is blocked temporarily and the material inside the formwork is still in a flowing consistency. If it is not possible to clean the lines and the old material in the lines has to be used, then the influence on the compressive strength could be more negative.

Tests 4 and 5 show the influence of a permanently blocked grout line and following grouting with a stinger from the top, similar to the contractor method. In general, no negative effect on the compressive strength was observed if no water is inside the formwork and no lubrication mix is used. Using a lubrication mix in the presence of water, an appreciable negative influence was detected.

General conclusion of the tests

The tests show a negative influence of ordinary lubrication mixes on the compressive strength of the test walls. The reduction of the compressive strength

occurs mainly in the upper and lower part of the walls.
The tests show a negative effect of 20 cm water inside the formwork when a lubrication mix is used. An intermix between grout, lubrication mix and water was found. A reduction of the compressive strength in the upper and lower part was observed here. When only grout without a lubrication mix was used, this phenomena was not noticed.
Without the overflow of intermixed grout material out of the formwork and without cutting 2 cm of weak material from the upper and lower parts of the test walls, the results would be more negative. Furthermore, the influence of a completely water-filled formwork on the compressive strength of the grout material could be more negative. Therefore, the findings of this first test show only tendencies and phenomena.
Amongst others, these aspects will be investigated in the project GROWup, funded by the Federal Ministry for the Environment, Nature Conservation and Nuclear Safety (BMU), Ref. No. 0325290.

References

[1] Welham, T.R.; Gilfrin, J.A.: “Installation of Grouted Pile-Sleeve Connections: A State-of-the-Art Review.” 25th Annual OTC, Houston, 1993.

[2] Lohaus, L.; Lindschulte, N.; Scholle, N.; Werner, M.: „Betontechnik für Grouted Joints – Baustoffliche und bauausführungstechnische An-forderungen.“ Stahlbau 81(2012), Heft 9.

[3] Lohaus, L.; Werner, M.: “Probabilistic Aspects of Offshore Wind Turbines: Influences of In Situ Assembly of Grouted Joints.” Life-Cycle and Sustainability of Civil Infrastructure Systems, CRC Press/Balkema, Leiden, 2013.

[4] Werner, M.: „Grouted Joints in Offshore-Windenergieanlagen – Materialverhalten hochfester Verguss-mörtel bei unplanmäßigen Ereignissen während des Verfüllvorgangs.“ Tagungsband zur 1. DAfStb Jahrestagung 2013, Bochum, 2013.

[5] Zement-Taschenbuch 1979/80. Bauverlag, Wiesbaden und Berlin, 1979.

[6] DAfStb-Richtlinie: Herstellung und Verwendung von zementgebundenem Vergussbeton und Vergussmörteln. Beuth Verlag, Berlin, 2011.

2.6 Monitoring of Mechanical Components (WP 6)

IMKT (Institute for Machine Design and Tribology)
Gerhard Poll, Roman Böttcher

In light of the turnaround in energy politics towards renewable energies, the number of installed wind turbines grew and will grow further in near future due to financial support e.g. in form of a compensation for electricity fed into the grid in Germany. It is already scheduled to decrease these subsidies for renewable energies in the future, so that wind turbines have to compete with the production of energy by help of fossil energy sources. To achieve lower costs, wind turbines and their power will grow for sites with good wind conditions or will be optimized for locations with lower wind speeds to make best use of the natural resource wind. As a result, wind parks are built near and far offshore and the variance of different types and concepts of wind turbines grows according to a technical evolution.
To ensure an economic operation of wind turbines and especially of offshore wind turbines (OWT) with high availability and low maintenance costs, condition monitoring systems (CMS) are needed to detect failures in the drive train of wind turbines during operation reliably. The aim of work package 6 therefore is the development and optimization of monitoring and diagnosis systems that should be applicable to different types of drive trains in OWT and can also help to achieve basic knowledge during experimental studies on single components of the OWT drive train.

2.6.1 Motivation

Operation of wind turbines

Maintenance costs have the biggest share on the operation costs of wind turbines. Figure 1 shows the allocation of the operation costs for a wind turbine in Germany for the first half of the designed period of use and the second one on an average. It is shown, that the proportions of the categories of costs change between these two decades with a rising share of maintenance costs towards the end of the planned life time of the wind turbine. The maintenance costs do not only increase in relation to the other operation costs, their absolute value also grows. The operation costs therefore increase in the second decade for the proprietor of the wind

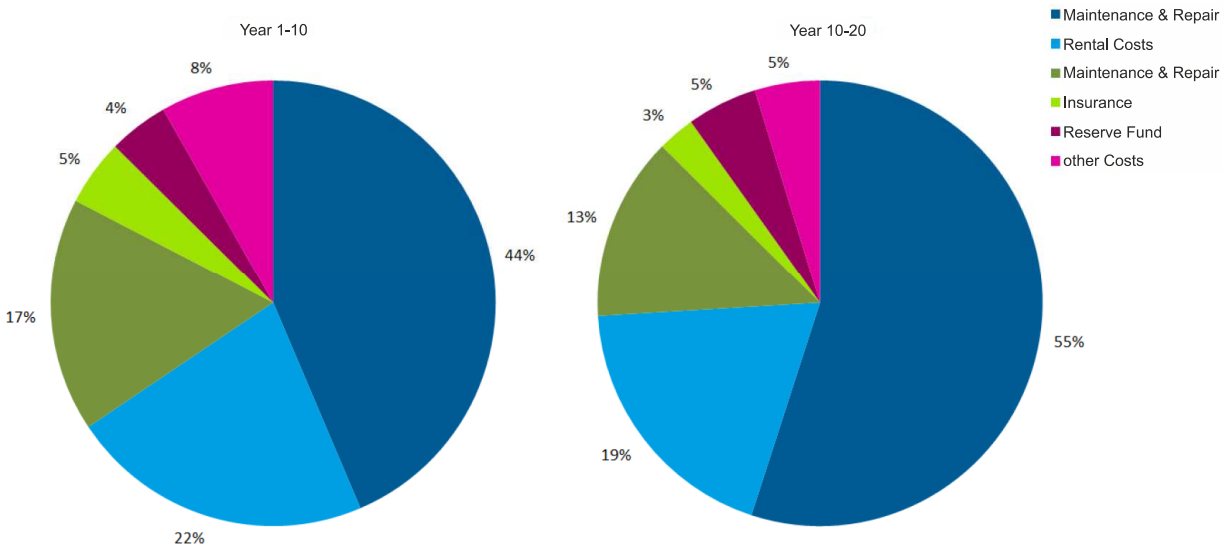

Figure 1: Amount of different categories of costs on the operation costs of wind turbines [1]

turbine, see [1]. A limited durability of the wind turbine parts, changing systems of maintenance and the influence of warranty given by the manufacturer in the first years of operation are causal for this change in the amount of maintenance costs.
[2] determines, that the share of maintenance costs on the operation costs are higher for a wind turbine operated offshore than those of an onshore turbine. Offshore wind turbines are naturally less well accessible then onshore turbines because of their location in open water. In addition maintenance and repair are made more difficult due to the fact that the turbines are inaccessible by ship for over half of the year because of critical wave heights above 1m, see [3] as an example for the German Bight. Therefore, failures of components are accompanied by higher costs for transport of material and staff for repair by ship or even helicopter and high costs for long downtimes.
While the capital costs per kW of power of a wind turbine including e.g. the expenses for manufacturing, transport and installation of the wind turbine and its infrastructure can be reduced by the development of bigger turbines and a further industrialization and optimization of the manufacturing and installation process, failures of drive train components and their costs for repair and maintenance cannot be necessarily avoided only through technical progress during development. Malfunctions of rolling element bearings due to fatigue as a result of the repetitive overrolling in operation occur even under ideal lubrication conditions and are typically distributed stochastically.
For the dimensioning of rolling element bearings, only a failure probability can be calculated. This calculation is based on a histogram that approaches the dynamic stresses loading the bearings over the lifetime of the wind turbine. This necessary simplification can cause incorrect assumptions because short time events, e.g. wind gusts on the wind side or short circuits on the electric side of a wind turbine cannot be taken into account as well as the sequence of the load distribution when calculating over an estimated life time of a turbine of 20 years. The influence of short time events on the lifetime of cylindrical roller bearings (CRB) was investigated during a research project at IMKT, see also [4]. As a result, short time events cannot be considered as causal for frequent failures in gear boxes of wind turbines. Endurance tests with different load steps even showed an increasing lifetime, when CRBs were exposed to initial high loads before testing with normal loads.
Another inaccuracy can already result from the choice of a wind distribution and the resulting load distributions for a wind turbine that has to be planned. Typical stochastic distributions can be developed originating from measurements on different sites, see for example [5]. However, the real load spectrum can differ during the long time of operation of the particular wind turbine.

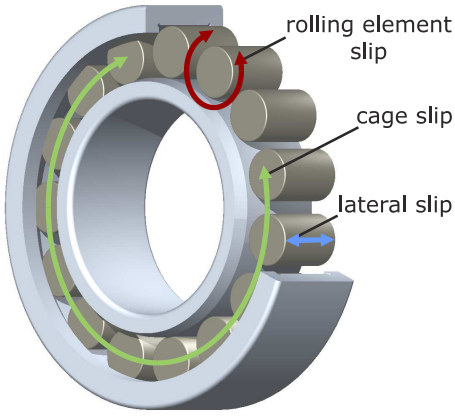

Figure 2: slip in rolling element bearings

There are other influences on the lifetime of rolling element bearings of wind turbines such as White Etching Cracks (WEC) and slippage that are not yet investigated sufficiently and therefore not even implemented in their lifetime prediction. WEC lead to early failures while the slippage of bearing parts – the divergence of the actual movement of

these parts to the motion predetermined by their geometry - leads to additional strains in circumferential direction in the rolling contact or even to smearing, which are changes in the surface of metallic bodies in relative motion with beginning adhesive wear, see [6].

Three slip conditions can be distinguished as shown in fig. 2. Lateral slip can occur due to tilting in CRBs or due to dynamic axial loads that displace the bearing parts in its axial clearance repeatedly. Slippage in circumferential direction of both rolling elements and cage respectively the whole rolling element set results from rotational accelerations of the bearing while the forces in the contact of rolling elements and their raceways aren't sufficient high enough to ensure a pure rolling motion.

To compensate uncertainties in the load assumption or in the calculation method while determining the lifetime of rolling element bearings for wind turbines, correction factors have to be used. Therefore there is a risk to oversize parts. This involves needless higher costs and can have negative effects on technical systems such as rolling element bearings. The risk of slip increases with growing bearing dimensions on account of an increasing mass-inertia of the bearing parts. Large size bearings of wind turbines are especially endangered to endure slippage by reason of their dimensions and non-stationary and non-controllable operation conditions.

Since it is not possible to calculate and guaranty the precise instant of failure of rolling element bearings and other components in the drive train of wind turbines, the condition of these components has to be monitored to ensure an operation with minimized downtime. By help of an early recognition of failures, maintenance can be planned early and effective. Downtimes with resulting financial losses and the maintenance costs itself can be reduced for the monitored wind turbine, especially if it is built offshore or even far offshore. An extensive and effective condition monitoring system collects data that can be used as a backflow of experience for further designs and the research of damage mechanisms. In addition, it helps to lower the yield risk of future wind plants and parks by an increasing of the availability, which improves the attraction of investors.

Condition Monitoring of Bearings in Wind Turbines

The condition of mechanical components can be monitored by different physical values. To give an example, the impermeability of a seal against water can be detected by a moisture meter, the structural integrity of a component by strain gages, displacement sensors or by the determination of its natural frequencies and their variation in case of a failure. While some of these methods provide information about the condition in a digital state – failed or intact – some others can also detect the variation of the particular value. Although it is useful to gain information about a variation of the condition, it is often also difficult to interpret correctly at which value of the particular physical quantity a failure can be defined. It is made difficult because differences in the properties of the particular component due to deviations in manufacturing, changes in operation conditions as well as interferences on the physical value, the sensor converting the physical value in an electrical signal and the transmission of this signal lead to changes in the measured value. Therefore, instead of the measured value, the rate of change is often used to detect failures.

To monitor the condition of rolling element bearings during operation, sensors are mostly used that shall measure the acceleration of vibrations caused by shock pulses. These shock pulses are emitted due to the repeated overrolling of the bearing raceways by the rolling element respectively damages on these parts. The drive train of a wind turbine contains

different elements that generate vibrations such as rolling element bearings and toothings.
The frequency of the pulse repetition depends on the geometry of the particular component, the damage location (e.g. inner ring, outer ring, cage or rolling element) and the rotational speed. The drive train of a wind turbine with a gearbox contains several rolling element bearings supporting the rotor and the shafts in the gear box and the generator. A gearbox is used to convert the slow rotational movement of the rotor into higher rotational speeds required by the generator. Since the size of the components generating vibrations and their rotational speed in the drive train of a wind turbine changes from the wind side to the electrical site, each component normally has different characteristic frequencies during operation. Therefore, a noticeable change in the acceleration signal and therefor a failure can be assigned to a particular toothing or even a single bearing part.
The design of wind turbines changes to achieve lower costs of energy. With the increasing power of the turbines and an increasing length of rotor blades, the drive train of wind turbines has to endure higher loads and has to be therefore larger and heavier. The mass of the drive train has to be supported by the nacelle, the tower and the foundation which have to get sturdier by themselves. To reduce the tower head mass, integrated drive trains were developed, where rotor and gear box as well as gear box and generator are connected directly without the use of intermediate shafts and are therefore lighter, see [7] for different types of drive train concepts. Due to the more compact construction, more rotating parts emit vibration signals in the housing of the gearbox, where the acceleration sensors are mounted normally. That makes it less easy to separate certain pulse shocks in addition to a modulation of the signal with other vibrations like additional components for the operation of the turbine (e.g. hydraulic pumps, actuators).
Further space savings and higher gear ratios for slower rotating rotors could be achieved by substitution of spur gears with planetary gears. Since planet wheels rotate around themselves and rotate with their carrier, shock pulses of damages in planetary bearings are difficult to detect with stationary acceleration sensors and conventional CMS-methods. These methods normally use low-pass-filters to separate an envelope curve with the interesting part of the signal from other vibration signals. Cut-off frequency, filter type and order of the filter have to be adapted for different rotational speeds and every gearbox. This approach requires that the modulated vibrations and the transmission behavior of the structural components are known and do not vary during operation and life time of the wind turbine. The envelope curve produced by filtering can be distorted due to transient response or overshoots. Therefore there is a risk that failures are not detected early or at all because of less optimal designed filters.
Therefore a condition monitoring system for the rolling element bearings in the drive train of wind turbines has to be developed, that works more reliable and that can be applied to modern drive train concepts.

2.6.2 Approach

A new type of analysis procedure as described in [7] shall be examined to prevent causes of error in the detection of bearing damages as a result of the difficulties as described in the previous chapter (variable speed, filter design, more compact drive trains). This method uses a Hilbert transformation to get an envelope curve without the usage of filters. The novel procedure of analysis was already tested successfully on a test rig for small CRBs with constant load and rotational speed. However, the conditions in OWTs impose special requirements.

Condition Monitoring of a large Size Bearing Test Rig

It was planned to evaluate the performance of the new analysis procedure on a large size bearing test rig that is operated by the IMKT. The rig was designed for experimental investigations with large size bearings under various conditions, especially those that may cause unexpected bearing damages or failures in practical applications. Acceleration sensors were mounted on several positions of the rig, which contains one test bearing and three support bearings. A data acquisition system was set up and some scheduled test and even a beginning damage on the test bearing could be monitored by chance, although it was not a fatique damage, see [8].

Since it isn't supposed to perform life time tests on the large size bearing test rig, it is difficult to determine the frequency-weighted level of acceleration of real fatique damages during scheduled tests. Therefore, another test bearing was acquired, that is kept available for tests with an aimed damage by scratching or the application of small welding seams.

Condition Monitoring of a Wind Turbine

In the meantime, an opportunity arose to perform measurements on a real wind turbine. The installation of sensors and a data acquisition system was given priority to the experiments in the test lab. The particular wind turbine was built in woodland with a hub height of 100 m and 1,5 MW of power. It has a partial integrated drive train, where main bearing, gearbox and generator are fixed separately on the nacelle. In a partial integrated drive train, the gearbox is used as the second bearing for the rotor shaft instead of a second bearing.

Fig. 3 shows a scheme of the drive train. The rotorshaft is supported by one main bearing (MB, spherical roller bearing) and the input shaft of the gearbox. The gearbox contains one planetary stage and two spur wheel levels. The planetary gear is supported by two cylindrical roller bearings (A1 & A2), each of the three planets contains two double-row CRBs (B). Each shaft of the spur gears (C, D and E) is supported by two CRBs for radial and one four point contact bearing for axial loads. The generator contains two deep grove ball bearings (G1 & G2).

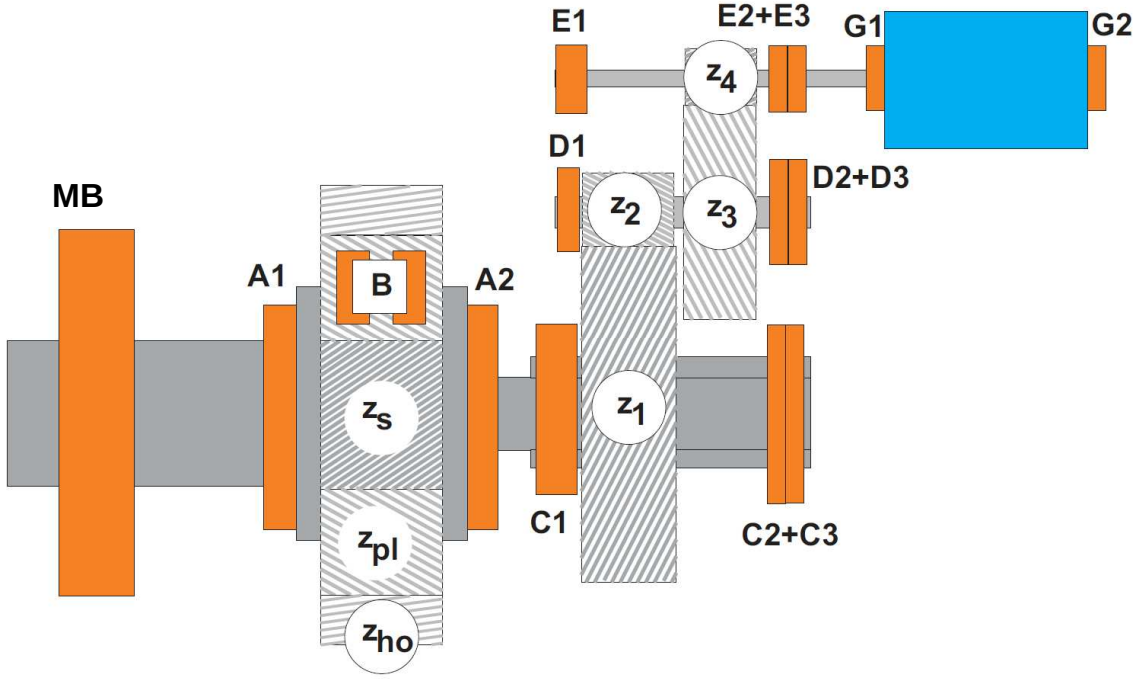

Figure 3: Drive train layout wind turbine for CMS-test

To measure the vibrations generated by the overrolling of the bearing parts and possible failures on their surface, two acceleration sensors were mounted radially on the generator, one for each bearing. Another four sensors were mounted radially on the gearbox; a seventh accelerometer is located axially on the generator side of the gearbox. To attach the acceleration sensors, mounting pads were bonded to the outside of the drive train components. The accelero-meters were threaded on them. The sensor positions were chosen in regard to the load direction of the bearings to detect the shock pulses in their direction of propagation if possible. While taking advantage of the transmission behavior of the gearbox housing, multiple rolling element bearings can be monitored with one accelerometer.

The eighth analog input channel of the data acquisition device is allocated to a laser distance sensor measuring the axial position of the gearbox that varies due to rotor thrust. It is supposed to use the eighth input channel for another acceleration sensor on the main bearing later as well.

While utilizing a condition monitoring system in serial application, system data such as wind speed, power and rotary speed of the generator can be received directly from the control system of the wind turbine. For our experimental setup and to be autonomous, own rotational speed sensors were installed using inductive and optical proximity switches and appropriate marks on the output shaft of the gearbox. With known transmission ratios of the gearbox, the rotational speed of each bearing can be calculated and utilized for an evaluation of the measured frequency spectrum regarding particular overrolling frequencies.

Figure 5: Wired data acquisition device

The data acquisition device as shown in figure 5 is operated stand-alone without the use of further computers on the wind turbine. Data, that is measured once a day, is saved on an internal storage and can be downloaded by help of a wireless data connection regularly. The installation and usage of a mobile network router was necessary since the data infrastructure was not sufficient and reliable enough. To

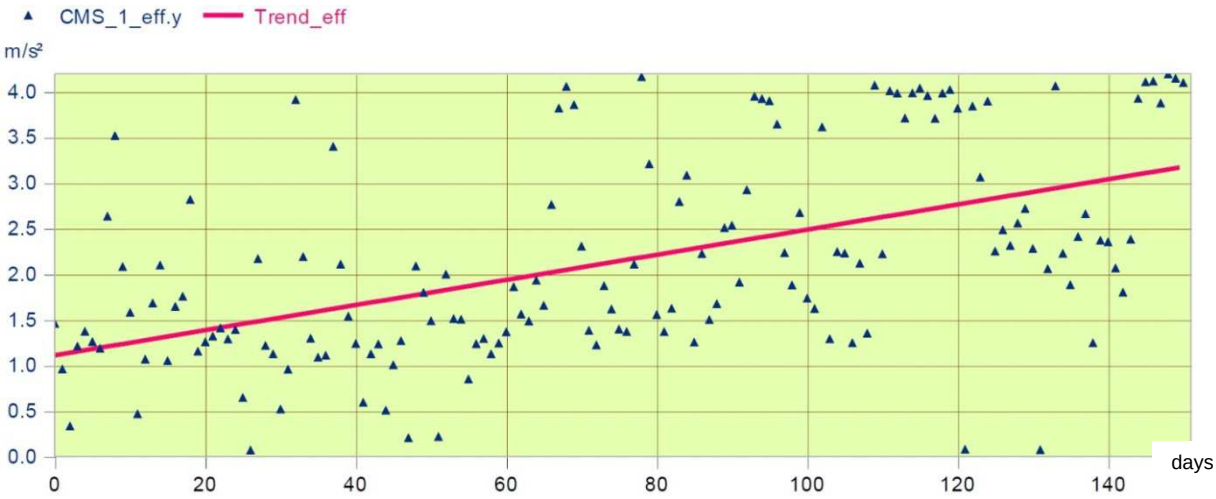

Figure 4: Development of the effective value of the acceleration measured with sensor 1

bypass power failures or power cuts and overvoltage that occur occasionally, an uninterruptible power supply was installed, too.

The installation and commissioning of the measuring technology started in spring 2013. Due to several difficulties regarding the infrastructure, the reliability of components and interfering influences, first data could be recorded in summer 2013. Figure 5 shows the development of the effective value of the acceleration measured with one of the radial sensors over a period of 150 days and its trend. An increase in the effective value can be seen, although it could be caused by an seasonal rise of wind speed –and a resulting rise of power and load–, too.

Fig. 6 shows two order spectra for the same sensor measured on two different days of operation with the same rotational speed. While operating with variable speed, the original vibration signal can be frequency modulated additionally. While using an order tracking analysis instead of a frequency spectrum, the problems induced by a frequency modulation can be evaded.

18.07.2013:

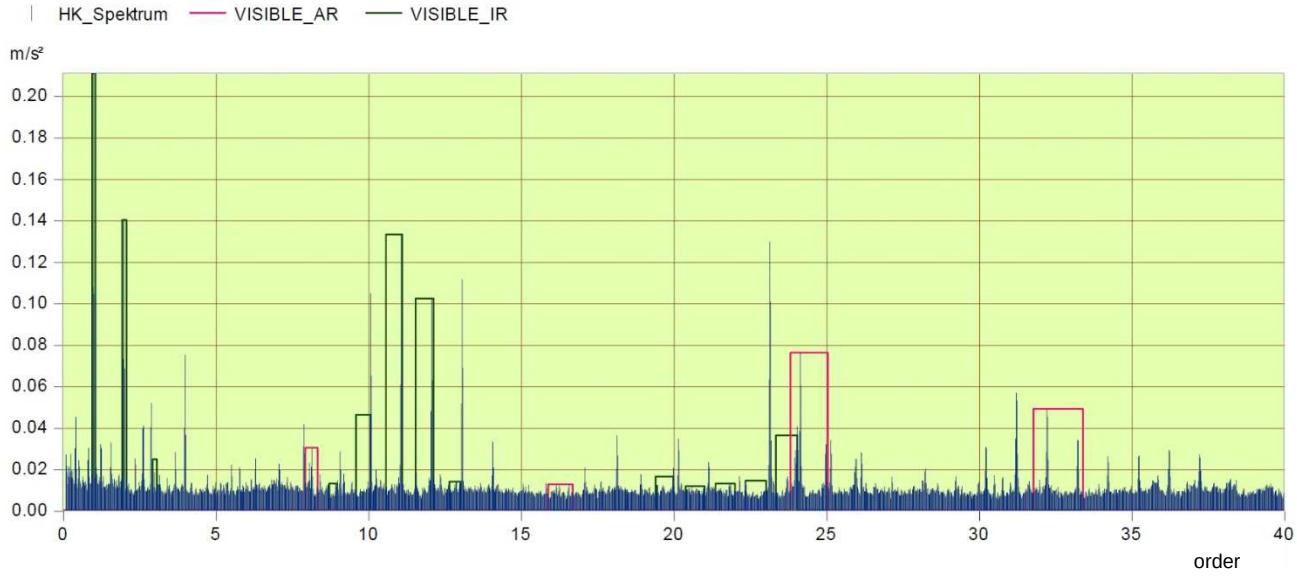

28.10.2013:

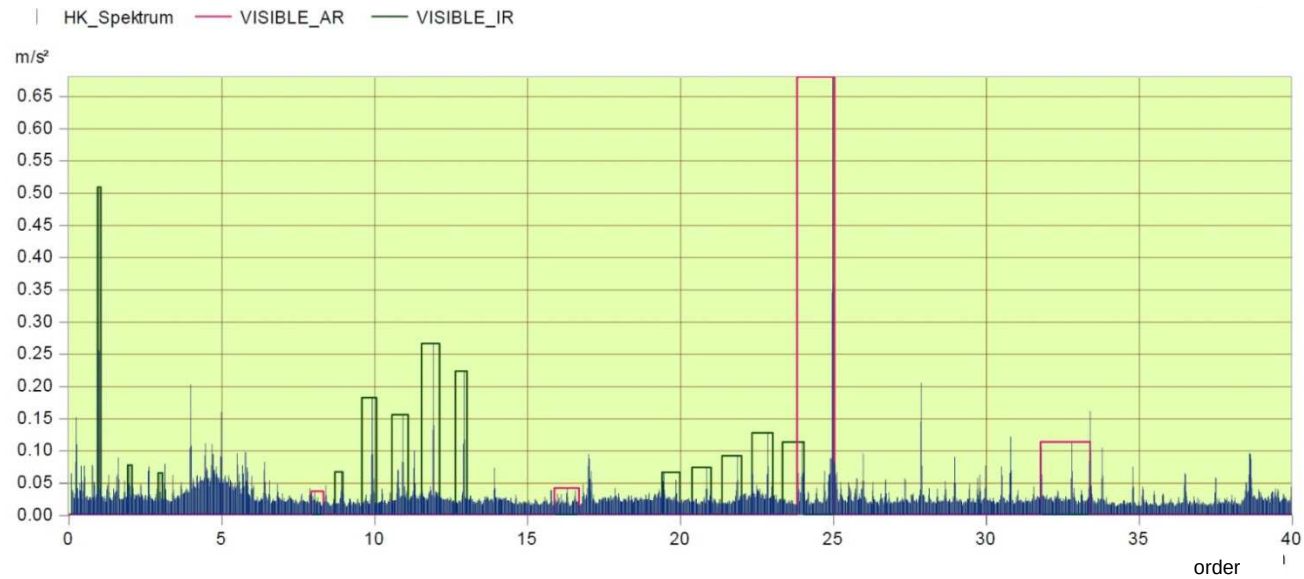

Figure 6: Order spectra based on measurements with acceleration sensor 1 on different days of operation

An order spectrum contains a distribution of accelerations over multiples of the rotational speed instead of frequencies in Hz. The measured signal transferred to an order spectrum by the analysis procedure as described in [7] is plotted in blue. The characteristic order of the outer ring and three of its related harmonic orders are marked magenta. The areas framed in green contain the rotational speed and two harmonics (order one, two and three) as well as the characteristic order of the inner ring (order 10,85), its harmonic order (order 21,7) and four sidebands (+/- one and +/- two orders) for each of them.
Considering the experience made with smaller bearings and the present experimental validation on the large size bearing test rig, the vibration levels don't seem to be high. Nevertheless, the pronounced appearance of the characteristic inner ring order with its harmonic orders and sidebands can already indicate an arising failure.

2.6.3 State of Work

Condition monitoring system

The operation of the wind turbine will be monitored further as well as the possible progression of a bearing damage on the high-speed shaft. If the vibration signal indicates a progression, pursuing actions will be performed by the operation company of the wind turbine that can be used as a validation of the condition monitoring system.
The collection of data and experiences will be used to develop an automated signal analysis and a simplification of installation and operation of the CMS.

Preload of screw connections

Work package six also contains the testing of experimental sensors to monitor screw connections and their forces during operation and over the life time of wind turbines. A sensor could be supplied in the meantime and the testing is currently performed.

References

[1] Rehfeldt, K.; Wallasch, A.-K.; Lüers, S.: Kostensituation der Windenergie an Land in Deutschland, survey for BWE and VDMA, Deutsche Windguard, 2013

[2] Arapogianni, A.; Moccia, J.: Economics of Wind Energy, Modern Energy Review, Vol. 4, Issue 2, 2012.

[3] Federal Maritime and Hydrographic Agency: Sea State for 2011, http://www.bsh.de/de/Meeresdaten/Beobachtungen/Seegang/S2011/Netz.jsp, Nov. 2012.

[4] Hacke, Radnai, Hinkelmann; Berücksichtigung von Betriebszuständen, Sonderereignissen und Überlasten bei der Berechnung der Wälzlager-Lebensdauer in Windenergieanlagen und Großgetrieben; Abschlussbericht FVA 541; Forschungsvereinigung Antriebstechnik e. V.; 2010.

[5] FINO – Research Platforms in the North Sea ansd Baltic Sea, http://www.fino-offshore.de/en/

[6] Hiltscher, G.: Anschmierung bei Wälzlagern – Ein Beitrag zur theoretischen und experimentellen Lösung des Problems, Phd. Thesis, Universität Nürnberg-Erlangen, 1989.

[7] Gasch, R.; Twele, J.: Wind Power Plants, Springer, Second Edition, 2012

[8] Hansen, M. et al.: Probabilistic Safety Assessment of Offshore Wind Turbines - Annual Report 2012

2.7 Diagnostic Systems for Electronic Systems (WP 7)

Institute of Drive Systems and Power Electronics
Meike Wehner

Due to the increasing number of installed wind turbines, early fault detection in wind turbine generators becomes more and more important. Especially in units with restricted accessibility like offshore wind turbines an early fault detection is necessary to avoid subsequent damages and long downtimes. WP 7 focuses on the online fault detection in electrical machines using search coil systems.

2.7.1 Motivation and Approach

All important types of faults and damages in electrical machines, such as winding faults, short-circuit faults or rotor eccentricities, result in characteristical changes of the magnetic air-gap field. These changes can be used to detect a fault by search coils placed in the stator slots based on the voltage induced in them to identify the type of fault in dependence of the frequency. Search coil systems are especially suitable for the detection of interturn faults and eccentricities, since these faults have no or little influence on the quantities at the terminals of a machine and are therefore not easy to be detected from the outside.
For an adequate condition monitoring system it is essential that the measured variable in case of a fault changes considerable compared to normal operation in order to avoid a false activation of the monitoring system. In theory, the sensor signals are assumed to be zero in faultless wind generators. In industrial applications, the signal fluctuations as well as the reachable signal-to-noise ratio have to be evaluated. On the other hand, the influence of the generator type and the power electronic components concerning reliability has to be researched. For this reason, two diagnostic systems will be dimensioned. Finally, the measured data are evaluated, and based on this, appropriate design criteria are elaborated for this kind of diagnostic systems.
For the application in wind energy plants, three generator types are in common use. Besides doubly-fed induction machines and salient pole synchronous machines, permanent magnet synchronous machines have been used more and more during the last years. Previous annual reports of WP 7 [1-3] describe the dimensioning of a search coil system for doubly-fed induction machines. Moreover it was determined in how far the detection of faults will be influenced by existing static or dynamic eccentricities.
In following the conclusions drawn from the search coil system of the doubly-fed induction machine are transferred to the dimensioning of search coil systems for permanent magnet synchronous machines with multi poles. Therefore a 3 MVA permanent magnet synchronous generator (rated voltage $U_N = 10{,}5$ kV, rated speed $n_N = 9$ 1/min, rated frequency $f_1 = 12\ Hz$), having 80 pole pairs on the rotor and 480 stator slots is determined. The resulting air-gap field and the voltages induced in case of a fault are analyzed based on rotating field theory by using the software ALFRED, which has been developed at IAL.

2.7.2 State of Work

The parasitic fields generated by the faults are detected by means of search coils placed in the slots of the stator core. The search coil system is designed in such a way that the reference parasitic field of the reference number of pole pairs ν_R, by which the respective fault shall be detected, induces with maximum amplitude, whereas the spatial harmonics in the air-gap field of the machine during normal operation do not induce any voltage in the search coil system. This is especially valid for the machine's

fundamental field of the number of pole pairs p.

The induced voltage strongly depends on the fault position, i.e. on the position of the shorted turn or the narrowing of the air gap respectively, towards the position of the search coil. To reduce this dependency, two identical search coils are used, and the resulting induced voltage $\underline{U}_{res}$ is split up by the use of the symmetrical components, the so-called positive- and negative sequence component $\underline{U}_m$ and $\underline{U}_g$, in two circular fields of the same frequency rotating oppositely towards each other. With the voltages $\underline{U}_{ia}$ and $\underline{U}_{ib}$ induced in the search coils a and b, splitting is made according to the relation

$$\underline{U}_m = \frac{1}{2} \cdot \left(\underline{U}_{ia} + j\underline{U}_{ib}\right) \quad (1)$$

$$\underline{U}_g = \frac{1}{2} \cdot \left(\underline{U}_{ia} - j\underline{U}_{ib}\right) \quad (2)$$

The complete calculation of the spatial harmonics in the air-gap field in synchronous machines during normal operation and in case of a fault was explained in detail in [4]. Moreover, criteria for the design of search coil systems for synchronous machines were described. One design condition based on these criteria is that the stator slot number is a multiple of

$$\widetilde{N}_1 = 2\,\nu_R \quad (3)$$

High-pole permanent magnet synchronous machines

In recent years the application of direct driven permanent magnet synchronous generators with large number of poles in wind turbines increases. The design of search coil systems for these high-pole machines thus bears a special challenge. For 80-pole machines, fundamental fields of the number of pole pairs of $\nu_R = p \pm 1 = 79$ or 80 are excited in case of a fault, according to equation (3) leading to a minimum number of slots of the search coil $\widetilde{N}_1 = 2\,\nu_R = 158$ or 162. The investigated generator has a number of stator slots of $N_1 = 480$, so that there is no common divisor of N_1 and $\widetilde{N}_1$ to match with the slot number condition according to equation (3). For machines with high pole pair/slot number combinations, specific measures must be taken when designing search coil systems.

Among the faults occurring in stator winding, winding shorts are the most difficult ones to be detected. Interturn faults lead to high circular currents within one coil of the winding only, without influencing the behavior at the terminals of the machine. For example they cannot be detected based on the terminal voltage or current. The thermal influence of the short-circuit current has the potential to deteriorate or destroy the machines winding within minutes. Furthermore the appearing distortion of the air-gap field in case of an interturn fault is locally restricted. For this reason, a search coil is required detecting the whole air-gap field along the bore, in order to detect an interturn fault independent of its position with a minimum of conductors.

The selection of the reference number of pole pairs depends on the faults which shall be detected. In case of an interturn fault, all spatial harmonics of the flux density of the number of pole pairs

$$\nu = g \;\forall\; g \in Z \quad (4)$$

are generated. Eccentricities lead to permeance waves having the largest amplitude with order numbers

$$\nu = \tilde{\nu} \pm 1 \quad (5)$$

with $\tilde{\nu}$ characterizing the order numbers during normal operation. According to this a reference number of pole pairs of $\nu_R = p - 1 = 79$ is selected.

The selectivity of a search coil can be characterized by the winding factor. The aim of the design is to reach a winding factor near 1 for the reference number of

pole pairs v_R, while spatial harmonics during normal operation lead to a winding factor of zero, above all the fundamental field of the number of pole pairs p. The complex winding factor referred to the number of pole pairs is given by

$$\underline{\xi}_\nu = \frac{1}{2z_w}\underline{\zeta}_\nu \tag{6}$$

with the effective number of conductors

$$\underline{\zeta}_\nu = \sum_{i=1}^{z_w} e^{j\nu\varphi_{hi}} - e^{j\nu\varphi_{ri}} \tag{7}$$

It depends on the number of conductors z_w and the position of forward and return conductor φ_{hi} and φ_{ri} in the stator slots. As can be seen from equations (6) and (7), the winding factor is maximum at distances between forward and return conductors (called coil pitch W below) of

$$W = \left(\frac{1}{2} + g\right)\frac{N_1}{\nu_R} \quad \forall \quad g \in Z \tag{8a}$$

and minimum for

$$W = g \cdot \frac{N_1}{\nu_R} \quad \forall \quad g \in Z \tag{8b}$$

Since the search coils are placed into the slots of the stator winding, the coil pitch must be an integer multiple of one stator slot pitch. For the investigated generator and the selected reference number of pole pairs, this leads to an optimum coil pitch of $W = 240$ slots. For this slot pitch, the condition of equation (8b) is fulfilled for the fundamental number of pole pairs p, so that the fundamental field does not induce into the search coil.

According to [4], the two identical search coils, splitting the resulting induced voltage into positive- and negative-sequence component, are ideally shifted according to

$$\varphi_M = \frac{\pi}{2\nu_R} \tag{9}$$

by half of the pole pitch of the reference field. In this case, the forward conductor of the second system is below the maximum of the reference field's excitation curve. As shown in [5], it is unproblematic to use multiples of this shifting. Even for high-pole machines, shifting is thus possible as an integer multiple of one slot pitch. For the investigated generator, the first maximum of the field excitation reaching an integer slot position is $\varphi_M = g \cdot \frac{\pi}{2\nu_R} = 120$ slots. Figure 1 shows the conductors as they are distributed in the search coil system based on the above made considerations. The search coil system consists of two identical search coils with $z_w = 2$ turns each, a coil pitch of $W = 240$ slots, circumferentially shifted against each other by $\varphi_M = 120$ slots.

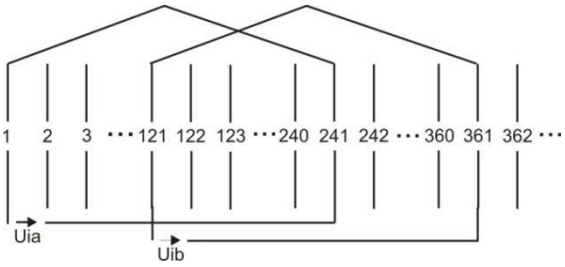

Figure 1: Distribution of conductors in the search coil system

Figure 2 shows the voltage induced in the search coil system for a shorted turn for different fault positions distributed along the circumference of the machine (given in slots). According to equation (4), the largest component of the induced voltage is induced by the spatial harmonic of flux density of the order number $\nu = 1$ with the frequency $f_\nu = f_1$. It can be seen that the induced voltage depends on the fault position. If the fault position is directly above the forward or return conductor of a search coil, the resulting voltage is zero. Considering the positive- or negative-sequence system, dips can also be observed at these positions, but the induced voltage at each position is large enough to ensure unambiguous fault detection. Besides the type of fault, it is

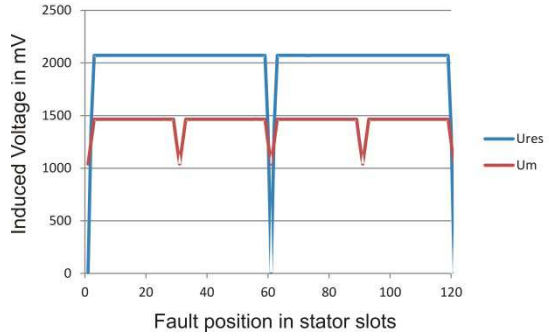

Figure 2: Voltage induced in the search coil system in case of an interturn fault for different fault positions

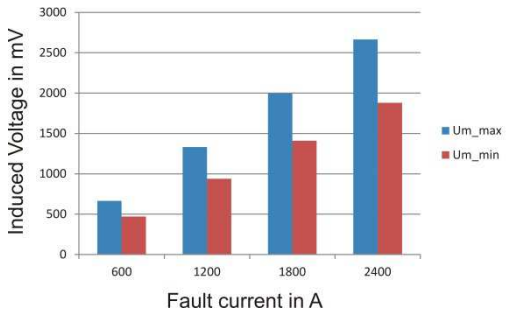

Figure 3: Minimum and maximum positive-sequence component of the induced voltage for different fault currents

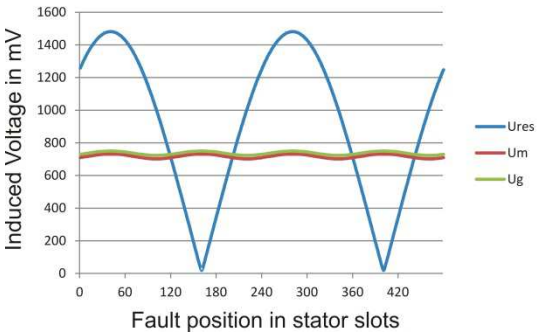

Figure 4: Induced Voltage in case of a static eccentricity of 30 %

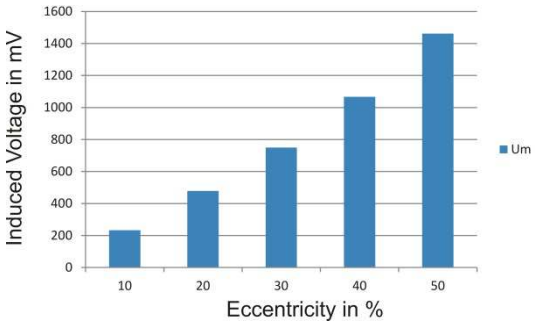

Figure 5: Positive-sequence component of the induced voltage for different levels of eccentricity

also desirable to evaluate the magnitude of the fault. As can be seen in figure 3, the induced voltage directly depends on the level of the short-circuit current, but is also influenced by the dependency of the fault position.

In case of a static eccentricity (index st) along the circumference of the machine, according to equation (5), the largest components of the induced voltage are induced into the search coil system with the number of pole pairs $v_R = 79$ and the frequencies $f_v = f_1 \pm f_\epsilon$ with $f_{\epsilon,st} = 0$. Similar to an interturn fault, the resulting voltage strongly depends on the fault position. As shown in figure 4, the positive-sequence component is on the contrary nearly constant and can thus be used for fault detection. According to figure 5, the level of the induced voltage is a measure to evaluate the level of static eccentricity.

Separate search coil systems for each type of fault

As both interturn faults and static eccentricities results in the characteristic frequency $f_v = f_1$, unambiguous fault detection is problematic. To avoid this problem [5] proposes the use of two separate search coil systems, each for one type of fault. The search coil system designed for detection of eccentricities (called search coil system A below) consists of four coils, evenly distributed around the circumference as seen in figure 6. To avoid the induction effect of the field with fundamental number of pole pairs p, the coils are connected in series referred to figure 6. This results in conjunction with the selected coil pitch in an induced voltage which is assumed to be zero in normal operation. According to equation (9) an identical search coil system is shifted by $\varphi_M = 120$ slots.

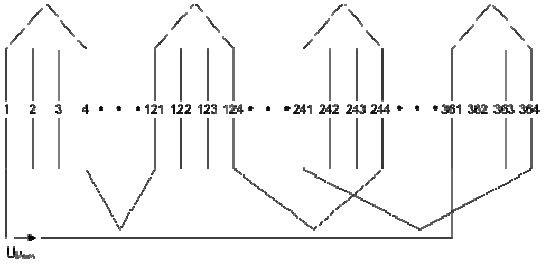

Figure 6: Winding distribution of search coil system A for detection of eccentricities

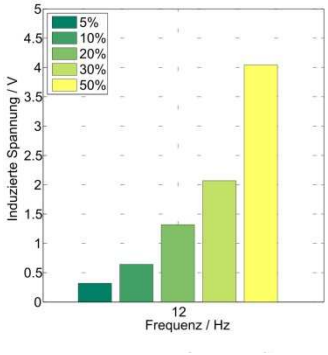

Figure 7: Induced Voltage of search coil system A for different levels of eccentricity

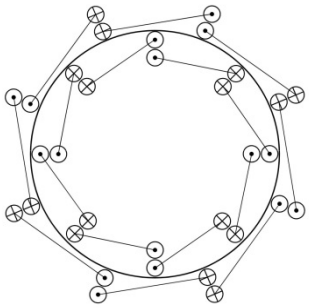

Figure 8: Winding distribution of search coil System B for detection of interturn faults

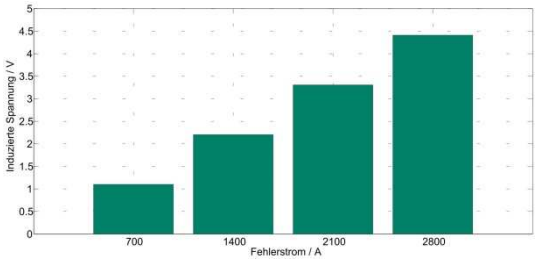

Figure 9: Induced Voltage of search coil System B for different fault currents

Figure 7 shows the voltage induced in the search coil system for different levels of eccentricity. Fault detection of interturn faults require detection the whole air-gap field along the bore. Hence the search coil system A is not suitable for detection of interturn faults independent of the position. A significant value of induced voltage is solely reached if the interturn fault occurs between forward and return conductors of one coil.

The second search coil system (called B below) is dimensioned for detection of interturn faults. As the fault detection should not be effected by eccentricities, the coil pitch is selected in such a way that the inducing effect of permeance waves due to eccentricity is largely eliminated. Purpose of the system B is to detect an occurring interturn fault with least number of coils independent of its position. Therefor the coil pitch is selected to $W = 60$ slots per coil. To cover the machines complete circumference, four search coils each with two adjacent coils are connected oppositional in series as seen in figure 8. As described before an identical search coil system is shifted around the circumference.

The main advantage of two separate search coil systems over the initially described system is unambiguous fault detection even if interturn faults and static eccentricities results in same characteristic frequency. Since the separate search coil systems are quite complex, however, a rotor-fixed search coil system is proposed in the following.

Rotor-mounted search coil system

The need for two identical search coil systems and the resulting duplication of conductors required arises from the dependency of the induced voltage on the

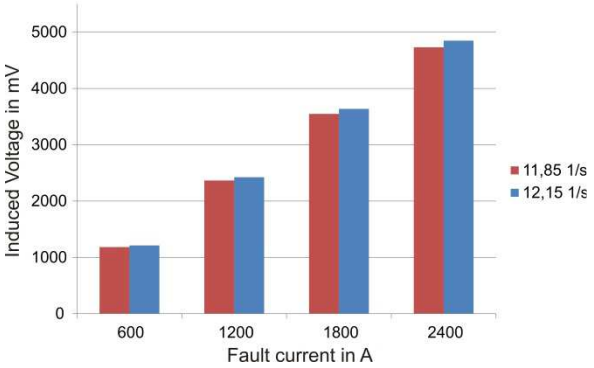

Figure 10: Induced voltage in case of an interturn fault and different fault currents for main frequency components

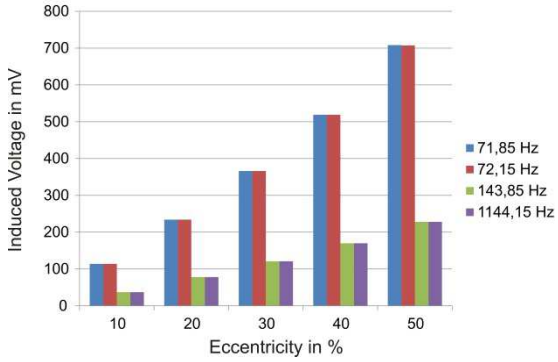

Figure 11: Induced voltage for different levels of eccentricity for main frequency components

fault position as well as on the characteristic component induced with the same reference frequency for different faults. To avoid these disadvantages, to minimize the complexity of the search coil system as well as to improve unambiguous fault detection in synchronous machines, a rotor-mounted search coil system is designed in the following. Since the coil rotates together with the rotor, it is not necessary that the search coil surrounds the machine's complete circumference. Moreover, the second search coil system can be ignored.
The frequency converted into rotor-fixed values is given by

$$f_{2,v} = f_v - n \cdot v \qquad (10)$$

with the rotational speed n. In case of an interturn fault in the stator winding, the largest value of the voltage induced in the search coil system is according to equation (4) induced for small order numbers v. With respect to (10) the stator-fixed frequency $f_v = f_1$ leads in the rotor to the characteristic frequencies

$$f_{2,WS} = 11{,}85 \text{ 1/s for } v = 1$$

$$f_{2,WS} = 12{,}15 \text{ 1/s for } v = -1.$$

According to figure 10, the value of the induced voltage is an ambiguous measure for the fault current level. Compared to a stator-fixed search coil system, the induced voltage does not depend on the fault position. In contrast to stator-mounted search coil systems, no search coil is required which surrounds the machine's complete circumference. It is sufficient when it covers just part of it, because the coil rotates together with the rotor.
In case of static eccentricities, the interesting number of pole pairs for a rotor-mounted search coil system are

$$v = -5p \pm 1 \text{ and } v = -11p \pm 1$$

with the corresponding frequencies

$$f_{(v=-5p+1=-399)} = 71{,}85 \text{ Hz}$$

$$f_{(v=-5p-1=-401)} = 72{,}15 \text{ Hz}$$

$$f_{(v=-11p+1=-879)} = 143{,}85 \text{ Hz}$$

$$f_{(v=-11p-1=-881)} = 144{,}15 \text{ Hz}.$$

According to figure 11, the value of the induced voltage is a measure for the level of eccentricity. Similar to an interturn fault, no dependency of the induced voltage on the fault position can be observed.
For rotor-mounted search coil systems, different faults thus lead to different characteristic frequencies. In this way, different faults can unambiguously be identified without the use of a second search coil system to observe the positive- and negative-sequence system.

2.7.3 Conclusion

Based on previous researches of search coil systems for synchronous machines, the special challenges of the design of

search coil systems for permanent magnet synchronous machines with high pole pair/slot number combinations are determined. In this respect different approaches for the design of search coil systems are presented.

References

[1] Wehner, M; Probabilistic Safety Assessment of Offshore Wind Turbines, WP 7, Annual Report 2010

[2] Wehner, M; Probabilistic Safety Assessment of Offshore Wind Turbines, WP 7, Annual Report 2011

[3] Wehner, M; Probabilistic Safety Assessment of Offshore Wind Turbines, WP 7, Annual Report 2012

[4] Ponick, B.; Fehlerdiagnose bei Synchronmaschinen. Dissertation, University of Hanover, 1994.

[5] Schroeder, H; Untersuchung von Messspulensystemen in permanent-magneterregten Synchronmaschinen zum Einsatz in Offshore–Wind-energieanlagen, Diploma Thesis, University of Hanover, 2013

2.8 Reliability of the Grid Connection (WP 8)

Institute for Drive Systems and Power Electronics (IAL)
Felix Fuchs

Institute of Electric Power Systems (IEE)
Stefan Brenner

Regarding the probabilistic safety of offshore wind turbines, the electrical system and the grid connection cannot be neglected. Together with WP 6 and 7, mechanical and electrical examination is covered.
The WP 8 is a collaboration between the Institute for Drive Systems and Power Electronics and the Institute of Electric Power Systems. The overall aim is to evaluate different grid connection topologies from the probabilistic point of view concerning the reliability. The two mentioned institutes are on the one hand specialized in the generator and its frequency converter and on the other hand in the grid connection itself.
The probabilistic reliability model of the whole electrical system will be implemented by the Institute of Power Systems, while the Institute for Drive Systems and Power Electronics delivers reliability models for power electronics and filter elements within the grid connection.

2.8.1 Motivation (IAL)

In studies of 2008, the most common cause of failure for wind turbines was found in the electrical part of the system [1]. More recent studies [2] show that this has not changed to this day. In particular, the converter is very often responsible for failures of the turbine. This further underscores the great need for research within the reliability of wind turbine converters.

2.8.2 Approach (IAL)

Within this project, an analysis concerning the lifetime of the converter of a wind turbine equipped with doubly fed induction generator (DFIG) has been done [3]. This was done for steady state operation as a first step. Afterwards, a dynamic model of the wind turbine was developed [4] with the aim of dynamic lifetime analysis. In 2013, this approach was further developed to analyse the dynamic lifetime consumption of the converter of a DFIG wind turbine.

2.8.3 State of Work (IAL)

The dynamic model of the DFIG wind turbine has been equipped with a wind speed profile which originates from the measuring point FINO in the german north sea [5]. Simulation results will be presented for the real wind speed step shown in Fig.1.

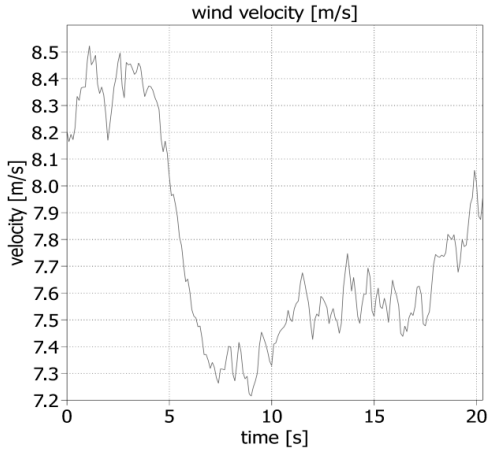

Figure 1: Wind speed step for crossing the synchronous operating point

In Fig. 2, an example plot of the wind speed measured in 80 m height of the FINO station can be seen.
The complete turbine simulation model cannot be run for a simulation time of one year due to the fact, that the simulation takes too much time. It is not possible to reduce the model so that it would be possible to simulate the desired one year operation. This is the reason why other approaches must be found to analyse the lifetime consumption of the turbine converter in dynamic operation. Here, a splitting of thermal cycles in different durations, e.g. in long term, medium term and short term intervals [6] and adequate

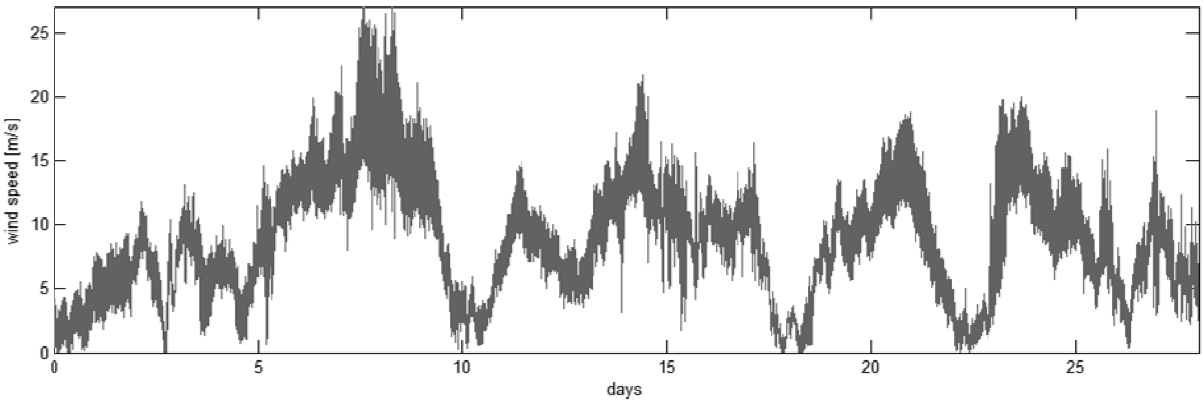

Figure 2: Wind speed at a height of 80 m at Fino 1 station in february 2006; time interval; one month

reducing of the model complexity results in a shorter and more realistic simulation time. This is also the aim of this work. Therefore first simulations are done with the example wind speed step shown in Fig. 1. This real speed step is interesting to analyse, because here, the DFIG turbine rotational speed reference crosses the synchronous operating point.

The simulation model is built in Matlab/Simulink/Plecs. The controllers for speed and current control are appropriately tuned. The power coefficient characteristic [4] of the turbine is included in the model. Also the speed control strategy based on the actual wind speed is integrated. Current and voltage limitations of the converter are respected. First simulation results are shown in Fig. 3. It can be seen that the synchronous operating point is crossed when the electrical frequency is near zero (at t=6s). Consequently, the junction temperature has higher delta T. When the wind speed drops to circa 7.5 m/s at t=7s, the electrical frequency increases again and so the delta T of the IGBT decreases. Near t=20s, the wind speed increases again to about 8 m/s and the turbine is again approaching the synchronous operating point.

The next steps of the project will be the application of model reduction methods as they are shown for example in [6] to speed up the lifetime simulation. After that the goal of lifetime prolonging operating strategies will be pursued.

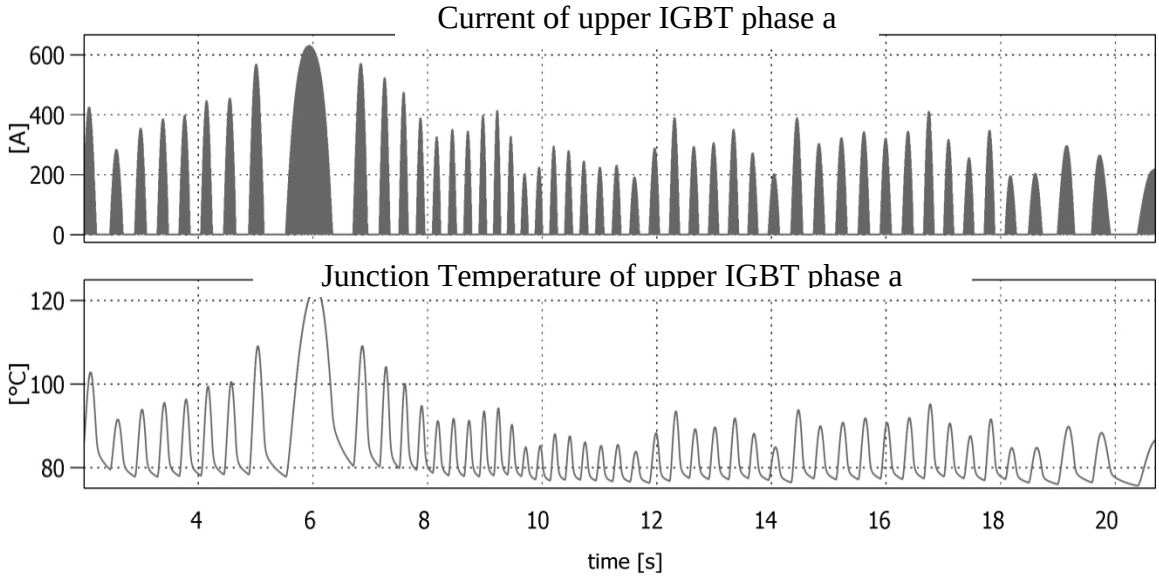

Figure 3: Current of IGBT and corresponding junction temperature for the wind speed step shown in fig.1

2.8.4 Motivation (IEH)

The operation and grid connection of large offshore wind farms in Germany is particularly challenging due to long distances of wind farms (WP) to the nearest point of common coupling as a result of protection of coastal areas and of the Wadden Sea. Long distances have to be bridged with submarine cables from the offshore substation to substation on land. In German North Sea, this is done usually as high voltage direct current transmission (HVDC).

Due to specific concepts a fault-free condition of wind farm grids is already a n-0 operation and counts thus as an endangered operation, considered with grid security standards of supply grids [13]. Due to the very poor accessibility of equipment, which is also strongly affected by weather, any possible damage, failure and its consequences must be considered in the project planning.

In order to consider the effects of the stochastically arising or time-variant environment effects such as wind, weather and aging of the equipment, reliability investigations with stochastic models must be developed. These must consider the influences of these parameters sufficiently exactly, in order to supply a possibility for the estimation of the probable failure behavior which can be expected with a desired dependability. For this problem various reliability analysis methods and methods for condition assessment are suitable. Depending on the objective both analytical and simulative methods are of choice.

A simulative method based on analytical considerations and a Monte Carlo simulation was developed to analyze all input parameters and status values. Furthermore the efficiency of offshore wind farms and the accessibility of them for repair and maintenance work are strongly depends on the prevailing wind speed. This dependence of reliability from wind speed distribution requires a modeling approach, which is provided by a wind time series model. This can then take influence on the reliability parameters and state variables of the equipment by various methods.

2.8.5 Approach (IEH)

The differential equation systems and their calculations are very complex in the analytical procedures. The reason for this is that systems with large number of components and increasing interaction of equipment among themselves become very complex. Although the methods provide very accurate results, but also require a high expenditure for the modelling of the overall system. Hence, simulation methods are often applied. These methods let a variety of freely distributed input parameters and provide a detailed analysis of the results, at this using a stochastic model [8]. In the simulation presented in this work based on a Monte Carlo procedure is a stochastic model (see Figure 4) used. With this model both the time of a failure und the duration during the outage can be considered. And additionally also modeled load curves of various parameters.

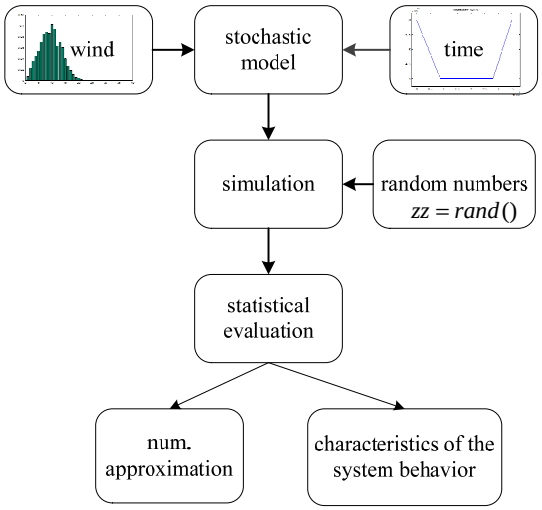

Figure 4: Principle of Monte-Carlo Simulation

For the reliability of a system, not only the stochastic or deterministic outage occurrences are significant. But also the effects of aging or mechanical stress that

can be considered as using different load scenarios are of importance. For the failure distribution stochastic processes such as wind supply and aging in a wind park are taking into account. For this, the Monte-Carlo procedure is very well suitable.

2.8.6 State of work (IEH)

Maintenance

An exact analysis of respective availability of the maintenance crews and individual location-dependent risk estimate of the weather conditions is badly feasible in a simulation. Due to the many different factors influence these variables. Therefore, a scattering of repair times is realized according to the maintenance model in Figure 5 by a direct coupling to the wind distribution. This returns the bad accessibility of the offshore wind farms (sometimes not more than 60 % of the year [9]), due to the weather conditions.

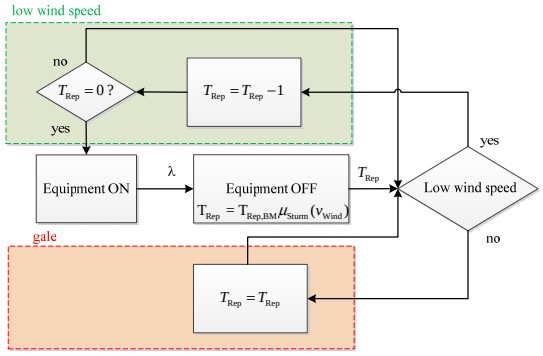

Figure 5: Model of the repair times in dependence of the wind velocity

The maintenance model, developed in this work puts the repair time T_{rep} of the failed equipment into a counting vector. The repair time determined in advance in case of failure and first applies a normal case. In each interval step (corresponding to 15 minutes) with low wind this repair or maintenance time is decremented 'Equipment is being repaired'. In case of a gale, where the wind speed is exceeds the specified limit of wind speed, the registered time to repair is not processed "*Equipment will not be repaired, due to gale*" (see Figure 5).Thus, the repair may be significantly extended during *gale* times. Thus the stochastically occurring serious failures, as well as the long-lasting repair and maintenance durations witch are relevant in practice can be simulated depends on the wind speed.

Gale model

High wind speeds produce strong mechanical and in particular high electrical stress for the wind energy generators [10]. Therefore, the blades of wind energy plant propeller will be feathered to stop the rotor during too high wind speeds (pitch-control) or the airflow through the blades will be changed by turning the blades (storm-control). A failure at high wind speeds is not only more probable due to the high stress, but if an error occurs the damage is more significantly. In this case longer repair times are to be taken into consideration and, hence, a partition in light and heavy damage categories is sensible.

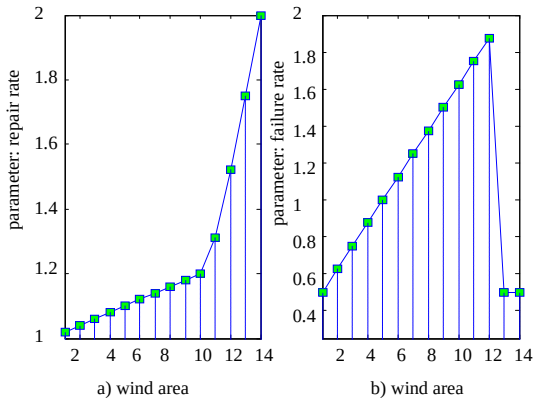

Figure 6: gale modeling for increased a) repair and b) failure rate

Hence, two models were developed (see Figure 6). The models describe a defined parameters depending on the wind speed at any time. The described parameters are, for example, the duration of an outage (see Figure 6 a) or factors for use in the maintenance model (see Figure 5). This permits a very exact distinction of the damage classes. The simultaneous conditioned increase of the failure probability became by a linear increase

Figure 6 b with consideration of the turn-off speeds with very high wind stresses depending on the wind energy plants. The single unities of the wind energy plants show very different failure dependence with increasing wind speeds [10]. Therefore, the model includes an averaging of the various correlations between the wind and the damage frequency of every asset component.

References

[1] ISET Kassel; Windenergiereport 2008 (in german).

[2] Wilkinson, M.; Harman, K.; Hendriks, B.; Spinato, F.; van Delft, T.; Garrad, G. L.; Thomas, U. K. (2011): Measuring Wind Turbine Reliability, Results of the Reliawind Project. In EWEA Conference (pp. 1-8).

[3] Fuchs, F.; Mertens, A.: "Steady state lifetime estimation of the power semi-conductors in the rotor side converter of a 2 MW DFIG wind turbine via power cycling capability analysis," Power Electronics and Applications (EPE 2011), Proceedings of the 2011-14th European Conference, vol., no., pp.1,8, Aug. 30 2011-Sept. 1 2011

[4] Fuchs, F.; Mertens, A. (2012): Dynamic modeling of a 2 MW wind turbine for converter issues: part 1, Power Electronics and Motion Control (EPE PEMC 2011 ECCE Europe), Proceedings of the 2012-15th International Conference and Exposition on, Novi Sad, Serbia

[5] Neumann, T.: “Erste Betriebs-erfahrungen mit der Fino1-Forschungs-plattform in der Nordsee (in german),” in DEWI Magazin, 2004, 2004.

[6] Ke, M.; Liserre, M.; Blaabjerg, F.: "Lifetime estimation for the power semiconductors considering mission profiles in wind power converter." Energy Conversion Congress and Exposition (ECCE), 2013 IEEE. IEEE, 2013.

[7] Hühnerbein, B.: Probabilistische Leistungsflussberechnung als Methode zur Bewertung der Einflüsse stochastischer Erzeuger und Verbraucher auf die Netzbelastung. Dissertation, Universität Hannover, 2010.

[8] Haubrich, Wellßow, Handschin, Seitz, Montebaur, Koglin. AKTR-Seminar Zuverlässigkeit. Mannheim-Rheinau : Forschungsgemeinschaft für Hochspannungs- und Hochstromtechnik e.V., 1994.

[9] Gasch, R.; Twele, J.: Windkraftanlagen: Grundlagen, Entwurf, Planung und Betrieb. Teubner Verlag, 2007.

[10] IWES, Fraunhofer Institut für Windenergie und Energiesystemtechnik. Abschlussbericht für das Verbundprojekt „Erhöhung der Verfügbarkeit von Windkraftanlagen“ .

[11] F. C. Sayas, R. N. Allan. Generation availability assesment of wind farms. Manchester : IEEE, 1996.University Science, 1989.

[12] Niesen, S.: Probabilistische Sicherheitsbewertung von Betriebsmitteln für Offshore-Windenergieanlagen. Hannover. Universität Hannover, 2010.

[13] R. Billinton, R. N. Allan. Reliability Evaluation of Power Systems. New York: Plenum Press, 1996.

3 Summary

Institute of Concrete Construction
Michael Hansen, Boso Schmidt

In the current reference period several analytical, experimental and numerical investigations of the structural design, different mechanical components as well as electrical machines and grid topologies of OWT are carried out. Hereinafter, essential investigations of the different WPs and their results are summarized.

The connections between the involved institutes and the unification of used reliability methods are focused in WP 1. In bilateral discussions the proceedings in each WP were evaluated to unite the methodology in all WPs. Thus, within WP 1 possible similar works of the several WPs are detected. The persons dealing with these WP obtain benefits by comparing their proceedings. Furthermore, a networked presentation of results of this comprehensive research project in reviewed papers is in progress.

In the first part of WP 2 the wave-breaking probability is investigated by means of laboratory experiments in two-dimensions to quantify the scatter of influencing factors. The first set of test runs showed a significant influence of the random phase angle on the number of breaking waves. For a better understanding of the sensivity of the random phase angle, test runs with a systematic relation of this parameter will be conducted. Furthermore, test runs with variations of the remaining influencing factors, namely the peak periods and water depths will be carried out.

In the second part of WP 2 the effect of structural uncertainties in rotor blades of OWT on the full-system mode shapes and natural frequencies of an OWT is investigated. To achieve this, the distributed blade mass density (BMassDen), the cross-sectional flapwise (FlpStff) and the edgewise stiffness (EdgStff) are varied relatively with respect to the corresponding baseline parameters. It is found out that the effect of local variances can be compensated, which only leads to small variations of the eigenfrequencies. In terms of spatial correlated variations of parameters an increasing correlation length leads to an increasing coefficient of variation.

In WP 3 a case study of a Reliability Based Design (RBD) of axially loaded piles for two common soil profiles and two design methods, the API-method and the ICP-method, is presented. It generally can be assumed that the calculated safety is in the range between a reliability index of 3,5 and 4,1. Also it was found out that the variation for the resistance arises mainly from the model error and that the soil uncertainty is less effective than expected. Based on the investigations, recommendations for the adaption of partial safety factors are given.

In WP 4 limit states which are critical for the structural design of the tower and substructure of OWTs are identified. The ultimate bearing capacity for axially loaded piles is investigated in detail. Therefore, probabilistic analysis with scattering wind and wave loads are conducted at a pile-modell with rigidly restraint or hinge support. Furthermore, the fatigue damage is investigated concerning its statistical properties. Scattering load parameters resulting from the environmental conditions are considered within the ongoing reliability analyses of the structural design of OWTs, too. . In addition to previous studies first statements on the correlation between significant load parameters are made.

The risk factors of the grouted joints during the execution process are evaluated in WP 5. Therefore, experimental investigations of the grout process are carried out. The tests show a negative influence of ordinary lubrication mixes on the compressive strength. The reduction of the compressive strength occurs mainly in the upper and lower part of the test specimens. If a lubrication mix is used a negative effect of water inside the

formwork could be detected. Without a lubrication mix this phenomena was not noticed.

Condition monitoring systems (CMS) are needed to detect failures in the drive train of wind turbines during operation. WP 6 deals with the development and testing of condition monitoring systems for large size rolling element bearings on a large size bearing test rig as well as on a real wind turbine. The collection of data and experiences is used to develop an automated signal analysis and a simplification of installation and operation of the CMS. WP 6 contains the testing of experimental sensors to monitor screw connections and their forces during operation and over the life time of wind turbines, too. A special sensor was supplied and the testing is currently performed.

WP 7 focuses on the online fault detection in electrical machines using search coil systems. The investigations bases on previous researches of search coil systems for synchronous machines. Special challenges of the design of search coil systems for permanent magnet synchronous machines with high pole pair/slot number combinations are determined. With respect to these former works different approaches for the design of search coil systems are presented.

The thermal behavior of the power electronics is modeled in the first part of WP 8. Simulation results show the dynamic thermal load of the converter for real wind speed steps.

In the second part of WP 8 different grid topologies and structures are evaluated concerning their reliability. By using simulation models the potential weaknesses of grid connections are identified. One result of these works is that the single unities of the wind energy plants show very different failure dependence with increasing wind speeds.

4 Literature

4.1 Publication List

4.1.1 Reviewed Articles

Lohaus, L.; Werner, M.:
Probabilistic aspects of Offshore Wind Turbines: Influence of in situ assembly of grouted Joints, Life-Cycle and Sustainability of Civil Infrastructure Systems.
CRC Press/Balkema, Leiden, 2013, pp. 2209-2213

Schmidt, B.; Göthel, O.; Göhlmann, J.; Grünberg, J.; Marx, S.:
Wellenbeanspruchung auf hydrodynamisch kompakte Betonstrukturen für Offshore-Windenergieanlagen.
Beton- und Stahlbetonbau 109 (2014), Heft 4, S. 265-274

Werner, M. (2013):
Grouted Joints in Offshore-Windenergieanlagen – Materialverhalten hochfester Vergussmörtel bei unplanmäßigen Ereignissen während des Verfüllvorgangs.
Tagungsband zur 1. DAfStb Jahrestagung 2013, Bochum, November 2013, S. 347-354

4.1.2 Reviewed Conference Contributions

Ernst, B.; Seume, J. R.:
Modelling Structural Uncertainty of Wind Turbine Rotor Blades for Aeroelastic Investigations.
Seventh M.I.T. Conference on Computational Fluid and Solid Mechanics - Focus: Multiphysics & Multiscale, June 12-14, 2013, Massachusetts Institute of Technology, Cambridge, MA 02139 USA

Ernst, B.; Seume J. R.:
Investigation of Structural Uncertainty of Wind Turbine Rotor Blades.
6. Dresdner Probabilistik-Workshop, 10. - 11. Oktober 2013, Technische Universität Dresden

Neubauer, T.:
Wälzlager und Betriebsfestigkeit. FVA-Seminar „Betriebsfestigkeit in der Antriebstechnik“ der Forschungsvereinigung Antriebstechnik e. V., 3.-4.12.2013, Mannheim

Neubauer, T.; Poll, G.; Denkena, B.:
Untersuchungen einer Lebensdauererhöhung von Zylinderrollenlagern durch eine gezielte Modifikation der Randzone.
10. VDI-Fachtagung „Gleit und Wälzlagerungen“, 23.-24.04.2013, Schweinfurt

Neubauer, T.; Poll, G.; Denkena, B.; Maiß, O.:
Fatigue Life Extension of Rolling Element Bearings by Residual Stresses Induced Through Surface Machining.
5th World Tribology Congress 2013, 8.-13.9.2013, Turin (I)

Neubauer, T.; Poll, G.; Maiß, O.:
Einfluss des Eigenspannungszustandes auf die Ermüdungslebensdauer von Zylinderrollenlagerringen.
54. GfT-Tribologie-Fachtagung „Reibung, Schmierung und Verschleiß“, 30.9.-2.10.2012, Göttingen

Ottink, K.; Poll, G.:
Investigations into Protective Seals for Ball Bearings.
22nd International Conference on Fluid Sealing, 3.-4.12.2013, Düsseldorf

Schaumann, P.; Kelma, S.:
Probabilistic Design of Extreme Loads Acting on the Foundations - Piles of a Jacket during an 1-Year Storm.
Proceedings of 9th PhD Seminar on Wind Energy in Europe, Uppsala University Campus Gotland (Sweden), 2013

Schmoor, K. A., Achmus, M.:
On the validation of reliability and partial safety factors for axially loaded piles in dense sand.
4th International Symposium on Geotechnical Safety and Risk (4th ISGSR), Hong Kong, 4-6 December 2013

Wang, D.; Poll, G.:
Calculation of slip of the rolling bearings by applying a rheological model for lubricants.
9. Arnold-Tross-Kolloquium, 14.06.2013, Hamburg

Wang, D.; Poll, G.:
Prediction of Traction in EHL Contacts.
5th World Tribology Congress
2013, 8.-13.9.2013, Turin (I)

Wennehorst, B.; Poll, G.:
Modeling Radial Lip Seal Friction - A FEM-based Multi-Scale Soft Micro-Elasto-hydrodynamic Lubrication Approach.
5th World Tribology Congress 2013, 8.-13.9.2013, Turin (I)

Werner, M. (2013):
Grouted Joints in Offshore-Windenergieanlagen – Materialverhalten hochfester Vergussmörtel bei unplanmäßigen Ereignissen während des Verfüllvorgangs.
1. DAfStb Jahrestagung 2013, Bochum, November 2013

Wittek, E. C.:
Tribologisches Verhalten neuartiger Fuel Economy Öle in Wälzlagern.
Informationstagung 2013 der Forschungsvereinigung Antriebstechnik e. V., 26-27.11.2013, Würzburg, FVA Forschungsreport 2013

Wittek, E. C.; Smirnov, A.:
Wälzlagerermüdung bei Mischreibung in Abhängigkeit vom Schmierstoff.
Informationstagung 2013 der Forschungsvereinigung Antriebstechnik e. V. , 26-27.11.2013, Würzburg, FVA Forschungsreport 2013

4.2 Doctoral, Diploma, Master and Bachelor Theses

Bank, S.:
Experimentelle Simulation typischer bei der Bauausführung von Grouted
Joints auftretender Risiken.
Diploma Thesis
IFB April 2013

Bode, M.:
Korrelation von Wind- und Seegangsbedingungen am Standort FINO 1.
Diploma Thesis
IfMa December 2012

Diederley, J.:
Numerische Schädigungsuntersuchung an Spannbetontürmen für Windenergieanlagen infolge Ermüdung.
Diploma Thesis
IfMa June 2013

Ewert, C.:
Rechtliche Rahmenbedingungen bei der Installation von Offshore-Windenergieanlagen.
Project Thesis
IfMa November 2013

Kerßen, J:
Statische und konstruktive Bearbeitung einer Suction-Bucket Gründung aus Beton für Offshore-Windenergieanlagen.
Master Thesis
IfMa August 2013

Könecke, N.:
Bestimmung der Sensitivität von statistischen Extrapolationsverfahren für die Ermittlung von Extrembelastungen von OWEA.
Bachelor Thesis
TFD July 2013

Osterndorf, M. S.:
Vergleich des statischen und dynamischen Verhaltens einer Jacket-Gründungsstruktur unter Wellenbeanspruchung.
Project Thesis
IfMa August 2013

Spiegel, C.:
Bestimmung der Ausfallwahrscheinlichkeiten von Rotorblättern mittels FORM und SORM.
Master Thesis
TFD September 2013

Tomann, C.:
Versuche zur Bestimmung der Entmischungsneigung hochfester Mörtel mit optischen und thermografischen Verfahren.
Study Thesis
IfB September 2012